OVERLAP PARAMETERS AND HEXADECAPOLE-INDUCED TRANSITIONS IN H - Ar MIXTURES
2

CENTRE FOR NEWFOUNDLAND STUDIES

TOTAL OF 10 PAGES ONLY
MAY BE XEROXED

(Without Author's Permission)

SESHU BABU YERNENI

OVERLAP PARAMETERS AND HEXADECAPOLE-INDUCED TRANSITIONS IN H_2-Ar MIXTURES

BY
Yerneni Seshu Babu, M.Sc.,

A thesis submitted to the School of Graduate Studies in partial fulfillment of the requirements for the degree of Master of Science.

Department of Physics
Memorial University of Newfoundland
July 1986

St. John's Newfoundland

Permission has been granted to the National Library of Canada to microfilm this thesis and to lend or sell copies of the film.

The author (copyright owner) has reserved other publication rights, and neither the thesis nor extensive extracts from it may be printed or otherwise reproduced without his/her written permission.

L'autorisation a été accordée à la Bibliothèque nationale du Canada de microfilmer cette thèse et de prêter ou de vendre des exemplaires du film.

L'auteur (titulaire du droit d'auteur) se réserve les autres droits de publication; ni la thèse ni de longs extraits de celle-ci ne doivent être imprimés ou autrement reproduits sans son autorisation écrite.

ISBN 0-315-33642-0

ABSTRACT

The collision-induced enhancement absorption spectra of the fundamental band of molecular hydrogen in its binary mixtures with argon at 201, 273, and 296 K were recorded with a 2 m absorption cell for total gas densities up to 160 amagat for several base densities of H_2 on an infrared spectrometer equipped with a specially-constructed data acquisition system controlled by a microprocessor system. Binary and ternary absorption coefficients of the band have been determined from the measured integrated absorption coefficients. The experimental profiles were analyzed by assuming appropriate line shape functions and using the theoretical matrix elements of the quadrupole moment of H_2, and the characteristic half-width parameters δ_d and δ_c of the short-range overlap-induced transitions and δ_{q2} and δ_{q4} of the quadrupole-induced transitions have been determined. The half-width δ_c of the intercollisional interference dip increases with the total density ρ of the perturbing gas and is represented by $\delta_c = a\rho_b + b\rho_b^2$. The contributions of the overlap and quadrupolar induction mechanisms to the total absorption of the band have been also separated from the profile analysis. For H_2 – Ar collision pairs, the overlap parameters λ and ρ which represent the magnitude and the range, respectively, of the induced dipole moment and $\mu_{overlap}(\sigma)$, the overlap-induced dipole moment at the Lennard-Jones intermolecular diameter, have been determined.

Further experiments of the fundamental band of H_2 in H_2 – Ar mixtures at room temperature were performed for gas densities up to 520 amagat. From these experiments, the hexadecapole-induced transition $U_1(1)$ corresponding to the rotational selection rule $\Delta J = +4$ has been observed, which represents the first such observation of a U - branch transition in a H_2-foreign gas mixture.

Acknowledgments

I am deeply indebted to my supervisor, Professor S.P. Reddy for his willingness to discuss problems, and for his suggestions and advice during the entire research project. I thank him for his counsel, good humour and criticism, which have enlightened, stimulated and encouraged me.

I am grateful to Mr. C.T.W. Hsieh for his help in assembling the stepping motor control unit and for many helpful discussions during the experimental work. I also express my gratitude to Dr. P. G. Gillard for his help in modifying the original design of the microprocessor controlled data-acqusition-system and in computer programming (Appendix A in the thesis). I thank Carol Broderick, a fellow student, for typing the thesis manuscript with great care.

Thanks are also due to the School of Graduate Studies, Memorial University of Newfoundland for providing financial assistance, to the technical staff of the Physics Department for their cooperation in several aspects of the experimental set-up, and to my friends for their constant encouragement.

This work would not have been possible without the love, constant moral support, and patience of my parents.

Table of Contents

CHAPTER 1

INTRODUCTION

Isolated homonuclear diatomic molecules such as H_2 do not possess permanent electric dipole moments in their ground electronic states and hence do not give rise to allowed infrared spectra in their pure rotation and vibration-rotation spectral regions. However, transient electric dipole moments can be induced during binary or higher order collisions between these molecules or between them and some other (foreign) molecules. Their induced moments are modulated by the vibrational, rotational, and relative translational motions of the molecules giving rise to infrared absorption spectra. This collision-induced absorption (CIA) was first observed in the fundamental bands of O_2 and N_2 by Crawford *et al.* (1949) and in the fundamental band of compressed H_2 by Welsh *et al.* (1949). Since then, a great amount of experimental work has been done by several researchers on the CIA of H_2 in the pure gas and in binary mixtures with other simple gases over wide ranges of temperatures and pressures. A review of the experimental work done prior to 1971 on the CIA of H_2 has been given by Welsh (1972) and comprehensive bibliographies on the subject were compiled by Rich and McKellar (1976) and Hunt and Poll (1986). Van Kranendonk (1974) and Birnbaum *et al.* (1982) have reviewed the theoretical aspects of CIA. Recently Reddy (1985) has given a comprehensive review of CIA of the

vibrational spectra of the hydrogens.

It is convenient to express the induced dipole moment $\mu_{ind}(R)$ in a colliding pair of molecules, following Van Kranendonk and Bird (1951) by the expression

$$\mu_{ind}(R) = \mu_{ov}(R) + \mu_q(R) + \mu_h(R) ,$$

where R is the intermolecular separation, $\mu_{ov}(R)$ is the short-range, angle-independent electron-overlap induced dipole moment resulting from the distortion of the electron charge distribution, $\mu_q(R)$ is the long-range, angle-dependent quadrupole-induced dipole moment arising from the polarization of a molecule by the quadrupole field of its collision partner, and $\mu_h(R)$ is the intermediate-range hexadecapole-induced dipole moment resulting from the polarization of a molecule by the hexadecapole field of its collision partner. In 'the exponential – 4' model for the induced dipole moment proposed by Van Kranendonk (1958), the overlap- and quadrupole- induced parts have been considered with $\mu_{ov}(R)$ and $\mu_q(R)$ varying as exp(-R) and R^{-4}, respectively. The third part, i.e., $\mu_h(R)$, varies as R^{-6} (see, for example, Reddy *et al.* , 1980).

As far as the induced fundamental ($\Delta v = 1$) band is concerned, the overlap matrix element $\langle v=0 \mid \mu_{ov}(R) \mid v'=1 \rangle$ gives rise to single transitions $Q_{1\,ov}(J)$. (It is common practice in CIA to represent Δv, the change in vibrational quantum number v, by the subscripts 0, 1, 2, ... etc.). A remarkable feature of the overlap induction is the occurrence of a characteristic dip in the Q branch which was first observed by Crawford *et al.* (1950) in H_2 – foreign gas mixtures and later confirmed by Chisholm *et al.* (1952) at higher gas densities. Van

Kranendonk (1968) has explained this feature in terms of a destructive interference between the short-range induced dipoles in successive collisions. A detailed kinetic theory of the intercollisional interference dips in the Q branch has been given by Lewis and Van Kranendonk (1971; 1972 a,b,c) and Lewis (1976, 1983, 1985).

In the quadrupole induction mechanism, the strength of the induced dipole depends on the quadrupole matrix element $\langle vJ \mid Q \mid v'J' \rangle$ of a molecule and the polarizability (α) matrix elements of its collision partner and vice versa. For the induced fundamental bands the matrix elements of the isotropic part of the polarizability contributes to the absorption of the single transitions $O_1(J)$, $Q_1(J)$ ($J \neq 0$) and $S_1(J)$ and, if the absorption is in the pure symmetric diatomic gas, to the double transitions $Q_1(J) + Q_0(J)$ and $Q_1(J) + S_0(J)$. The anisotropy component (γ) of the polarizability of the molecules of the collision pair contributes to the absorption of the transitions mentioned above as well as to the transitions of the form $S_1(J) + S_0(J)$. But in the CIA spectra of the fundamental band of H_2 in $H_2 - X$, (where X = He, Ne, Ar, ... etc.), only single transitions $O_1(J)$, $Q_1(J)$, and $S_1(J)$ are of importance and no double transitions need be considered.

In the hexadecapole induction mechanism, the magnitude of the induced dipole depends on the hexadecapole matrix element $\langle vJ \mid H \mid v'J' \rangle$ of a molecule and the polarizability of its collision partner. This induced dipole $\mu_h(R)$ gives rise to the single transitions $U_1(J)$ ($\Delta J = +4$) and the double transitions

$Q_1(J) + U_0(J)$ in the CIA fundamental band of a pure symmetric diatomic gas. In pure H_2 these transitions, first observed by Gibbs *et al.* (1974) have been studied in detail by Reddy *et al.* (1980). Prior to the present work, no hexadecapole-induced transitions have been observed in H_2-foreign gas mixtures.

One of the main features that distinguishes CIA spectra from the allowed spectra is the broad half-widths of the lines. The width of a line is due to short duration of the induced dipole and the uncertainty principle, $\Delta E = h/2\pi\Delta t$ (Van Kranendonk, 1957). If $\vec{R}$ is the range of the induction mechanism and $\vec{V}$ is the relative velocity of a molecule with respect to its collision partner, then the collision duration is given by $\Delta t = |\vec{R}|/|\vec{V}|$. The width (in cm^{-1}) of the collision-induced line is therefore given by

$$\Delta\nu = \frac{\Delta E}{hc} = \frac{|\vec{V}|}{2\pi c\,|\vec{R}|}.$$

Because of the smaller value of $\vec{R}$ in the short-range overlap induction, the $Q_{ov}(J)$ components will be broader than the components arising from the long-range quadrupole induction. Also, the relative translational energy of the molecules can be approximated by $\frac{1}{2}mV^2 \approx \frac{3}{2}kT$, which gives a $\sqrt{T}$ dependence for the half-widths of CIA lines. In the enhancement absorption of the collision-induced fundamental band of normal H_2, all possible transitions in a $H_2 - X$ (where X is a monoatomic molecule) at room temperature, arising from the overlap and quadrupolar induction mechanisms are shown in Fig. 1. The hexadecapole-induced U-transitions corresponding to $\Delta J = +4$ are not shown in this figure. At room

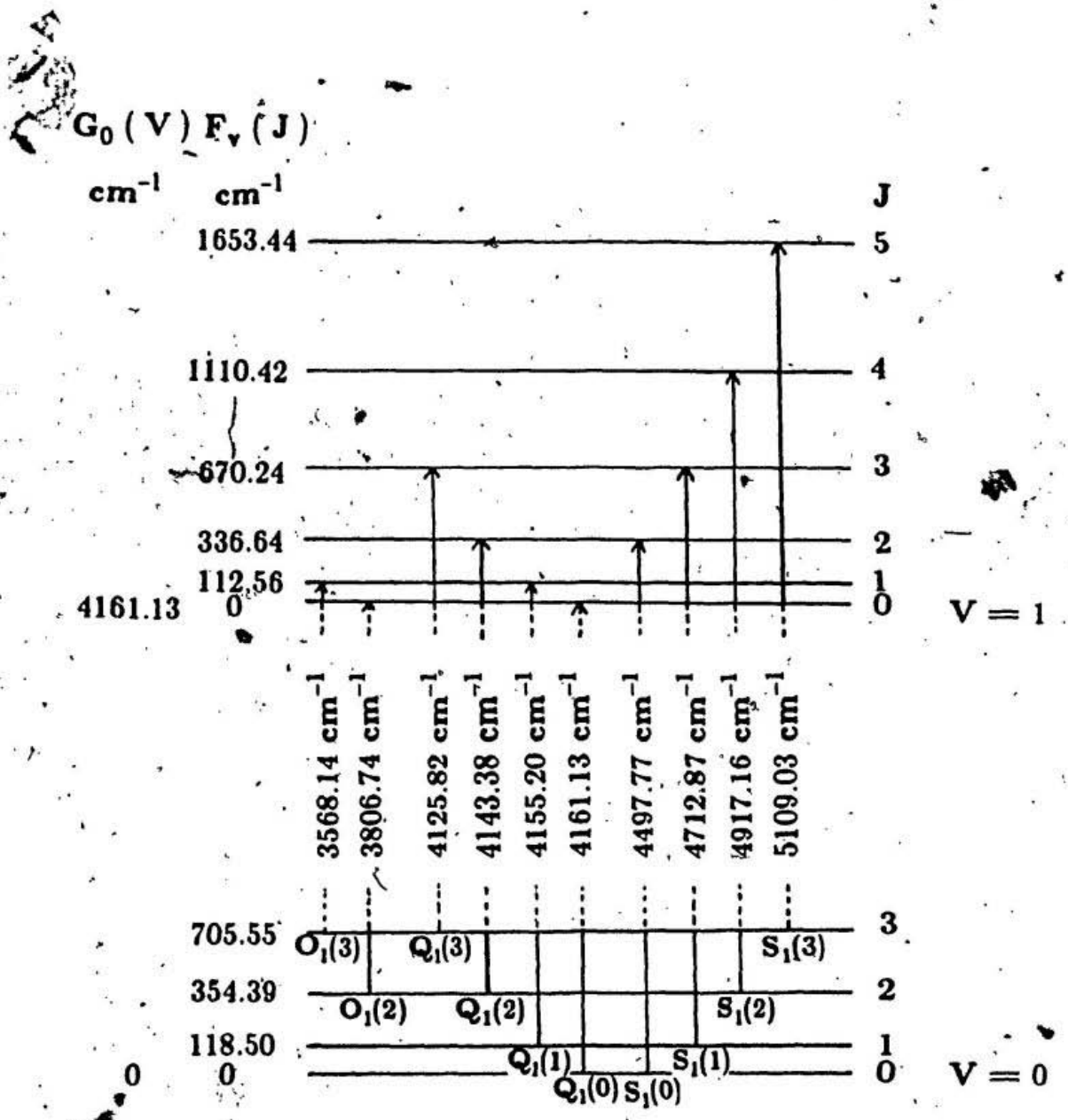

Fig. 1. Energy level diagram showing single transitions arising in the collision induced fundamental band of H_2 at 296 K.

temperature all the molecules of H_2 are distributed among the rotational levels J = 0 to 3 of the vibrational state v = 0. The vibrational terms $G_0(v)$ and the rotational terms $F_V(J)$ in Fig. 1 were calculated from the constants of the free H_2 molecule (Stoicheff, 1957). An enhancement absorption profile of the fundamental band of H_2 in $H_2 - X$ at room temperature contains a total of 13 components: two $O_1(J)$ (J = 2 and 3), four $Q_{ov}(J)$ (J = 0 to 3), three $Q_{1q}(J)$ (J = 1 to 3) and four $S_1(J)$ (J = 0 to 3).

The intensity of absorption of the collision-induced transitions depends not only on the matrix elements of the overlap induced moments and those of the quadrupole moment, hexadecapole moment, and polarizability, but also on the population of the initial states. The number of molecules N_J in a rotational state J of the ground vibrational level of a symmetric diatomic gas in thermal equilibrium at temperature T depends on (i) the (2J + 1) fold degeneracy (g_J) (ii) (2T + 1) fold degeneracy (g_T) due to nuclear spin and (iii) the Boltzmann factor $\exp(-E_J/kT)$, i.e., $\exp[-F_0(J)\,hc/kT]$. Here the absolute temperature T and the total nuclear spin T of H_2 should not be confused with each other. Since the nuclear spin of the H atom is 1/2, the total nuclear spin has 2I + 1 values, i.e., T = 1 (parallel spins) and 0 (antiparallel spins). Symmetric and antisymmetric rotational levels have even and odd T values, respectively. The ground electronic state of H_2 is $^1\sum_g^+$. Hence the even rotational levels J = 0, 2, ... are symmetric and have T = 0 (i.e., $g_T = 2T + 1 = 1$) and the odd rotational levels J = 1, 3, ... are antisymmetric and have T = 1 (i.e., $g_T = 3$). Thus

$$N_{J\ even} \propto 1\,(2J+1)\,\exp[-F_0(J)\,hc/kT]$$

and

$$N_{J\ odd} \propto 3(2J+1)\,\exp[-F_0(J)\,hc/kT]$$

Prior to the present work, some aspects of the CIA spectra of the fundamental band of H_2 in H_2 – Ar mixtures have been studied by previous researchers. The first observation of the band in H_2 – Ar was made by Crawford *et al.* (1950) at moderate pressures. Further observations on the band in H_2 – Ar was made by Chisholm and Welsh (1954) and Hare and Welsh (1958) at very high densities. A preliminary profile analysis of the band in H_2 – Ar was made by Hunt and Welsh (1964). Varghese *et al.* (1972) made an analysis of the profiles at room temperature in para H_2 – Ar mixtures. Mactaggart and Welsh (1973) and Mactaggart, De Remigis and Welsh (1973) studied the band in the normal H_2 – Ar and para H_2 – Ar mixtures at temperatures in the range 152 - 298 K and performed an analysis of the absorption profiles by appropriate line shape functions. However these authors did not obtain the overlap parameters such as λ, ρ and $\mu_{ov}(\sigma)$ for the H_2 – Ar mixtures.

The aim of the present research project was to make a systematic study of the CIA of the fundamental band of H_2 in H_2 – Ar mixtures for a number of gas densities at 201, 273, and 296 K, first by obtaining accurate absorption profiles and then by carrying out profile analysis by using line shape functions adopted successfully in the analysis of CIA spectra in the infrared. Another aim was to observe the U - transitions corresponding to the selection rule $\Delta J = +4$ and

arising from the hexadecapolar induction mechanism in H_2 - Ar mixtures. Details of the apparatus and experimental techniques are presented in Chapter 2. The enhancement absorption profiles of the overlap- and quadrupole- induced transitions and the derived absorption coefficients are presented in Chapter 3. The analysis of the absorption profiles and the results obtained therefrom are given in Chapter 4. The overlap parameters which characterize the induced overlap dipole moment μ_{ov} in H_2 - Ar collision pairs are determined in Chapter 5. Preliminary observations of $U_1(1)$ transitions in the CIA of the fundamental band of H_2 in H_2 - Ar are presented in Chapter 6. Finally, the conclusions of this research project are summarized in Chapter 7.

CHAPTER 2

APPARATUS AND EXPERIMENTAL TECHNIQUES

The enhancement absorption spectra of the collision-induced fundamental band of molecular hydrogen in its binary mixtures with argon were recorded for total gas pressures up to 160 atm at 201, 273, and 296 K for the overlap and quadrupole-induced transitions and up to 950 atm at 296 K for the hexadecapole-induced transitions. The experimental data were obtained with a 2 m high-pressure low-temperature absorption cell and an infrared recording spectrometer equipped with a data acquisition system and controlled by a microprocessor. During the present research project, several modifications were made to the data acquisition system and to the existing absorption cell. A description of the apparatus and its operation is presented in the present chapter.

2.1 The 2 m Stainless Steel Absorption Cell

A 2 m transmission-type stainless steel absorption cell originally designed for the experiments at room temperature by Reddy and Kuo (1971) and later modified for the experiments at low temperature by Gillard (1983) was used in the present studies after making further modifications and improvements. The cell, one half of whose cross-section is schematically shown in Fig. 2, was constructed from a type 303 stainless steel tube T, 2 m long and 7.62 cm in diameter. It has a central bore, 2.54 cm in diameter. A polished stainless steel light

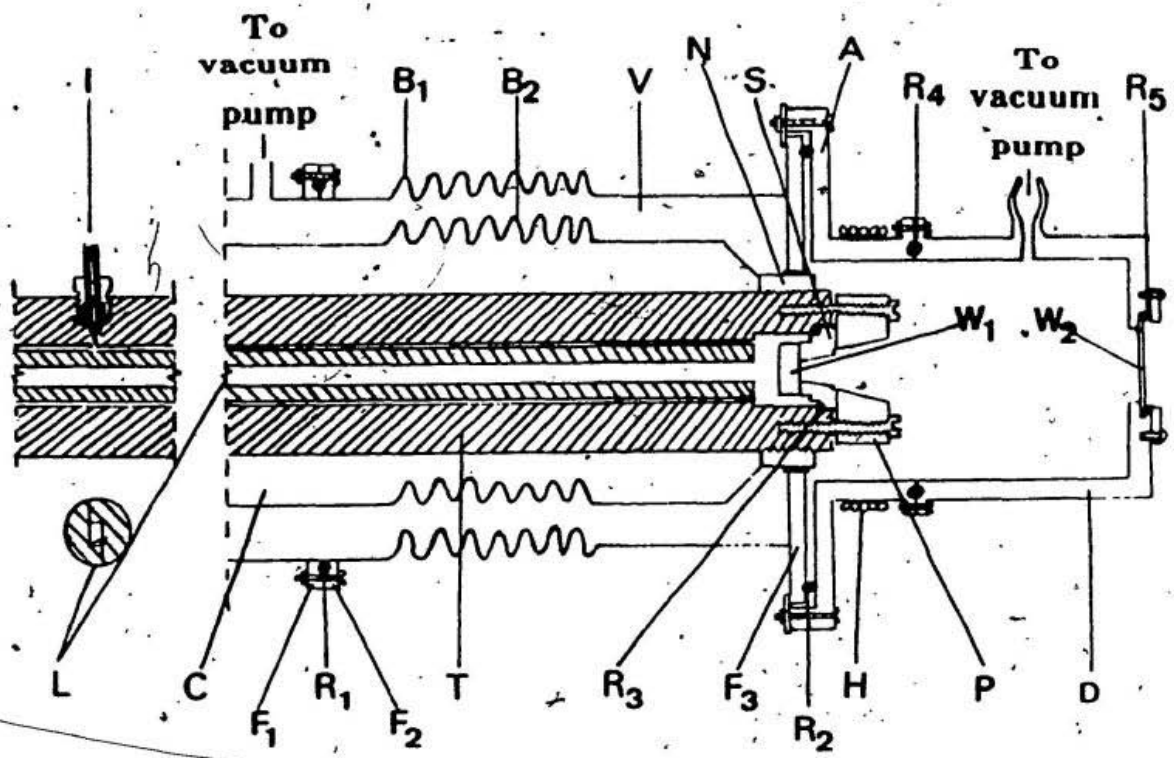

Figure 2 A cross - sectional view of one end of the absorption cell.

guide L with a rectangular aperture 1.00 cm x 0.50 cm, made in five sections and inserted into the bore ensured good transmission of radiation. A synthetic sapphire window W_1, 2.54 cm in diameter and 1.00 cm thick was attached to a window seat S having a circular aperture of 1.00 cm in diameter with General Electric RTV 108 Silicone Sealant. An inner O-ring R_3 between the window seat and the body of the cell was compressed by tightening eight Allen-head bolts against the retaining end piece P to obtain a pressure-tight seal. The experimental gases were admitted into the cell through an inlet I in an Aminco fitting.

A type 312 stainless steel nut N, 7.62 cm in internal diameter and 1.50 cm long was threaded on to the end of the cell and welded to it. A stainless steel flange F_3 and a stainless steel cone were welded to this nut. Eight holes were drilled in flange F_3 as illustrated in Fig. 2. A stainless steel bellows B_2, 10.2 cm in diameter was welded to the stainless steel cone. The outer jacket end piece consisted mainly of flanges F_1 and F_2 and bellows B_1 of 16.5 cm in diameter, all made of stainless steel. The two bellows allow relative expansion and contraction of the cell and the vacuum jacket V. A neoprene O-ring R_1 between F_1 and F_2 allows a vacuum seal. Chamber C was filled with an appropriate coolant.

Flange F_3 provided a seat for the aluminum end cap A which in conjunction with another end cap D made of Delrin material forms a vacuum chamber 10.0 cm long and 10.5 cm in diameter. The aluminum end cap was sealed against a silicone rubber O-ring R_2. A vacuum tight seal between the aluminum and Delrin end caps was provided by means of a neoprene O-ring R_4. A sapphire

window W_2, 5.08 cm in diameter and 0.30 cm thick, was sealed to the Delrin section with a neoprene O-ring R_3 between them. The vacuum chamber at each end of the cell was evacuated during the experiments to prevent frosting on the cell window. Heating tape H wound around the aluminum cap avoids freezing of the O-rings R_2 and R_4.

2.2 The Optical Arrangement and Spectrometer

The optical arrangement used in the present experiment is shown in Fig. 3. The source S is a 600 W General Electric FFJ quartzline lamp held in a water-cooled brass jacket and was operated at a voltage of 90 V, AC from a stabilized power supply unit. The radiation from the source was focused on the entrance window of the cell by a front coated concave spherical mirror M_1. The radiation leaving the cell was then focused onto the entrance slit of a Perkin-Elmer model 99 double-pass prism monochromator by a similar spherical mirror M_2. This radiation was collimated by an off-axis paraboloid mirror M_3 and then dispersed by an LiF prism P. The radiation was then reflected by the Littrow mirror to complete the first pass through the prism and brought to a focus. The diverging beam from this focus was chopped by a 260 Hz tuning fork chopper and sent back through the prism for a second pass. This radiation was then focused on an uncooled PbS detector. The wavenumber drum of the monochromator was coupled to the Littrow mirror. Thus the spectral region of interest could be scanned by rotation of the drum. The slit width maintained at 45 μm gave a spectral resolution of $\sim$5 cm^{-1} at the origin (4161 cm^{-1}) of the fundamental band of H_2.

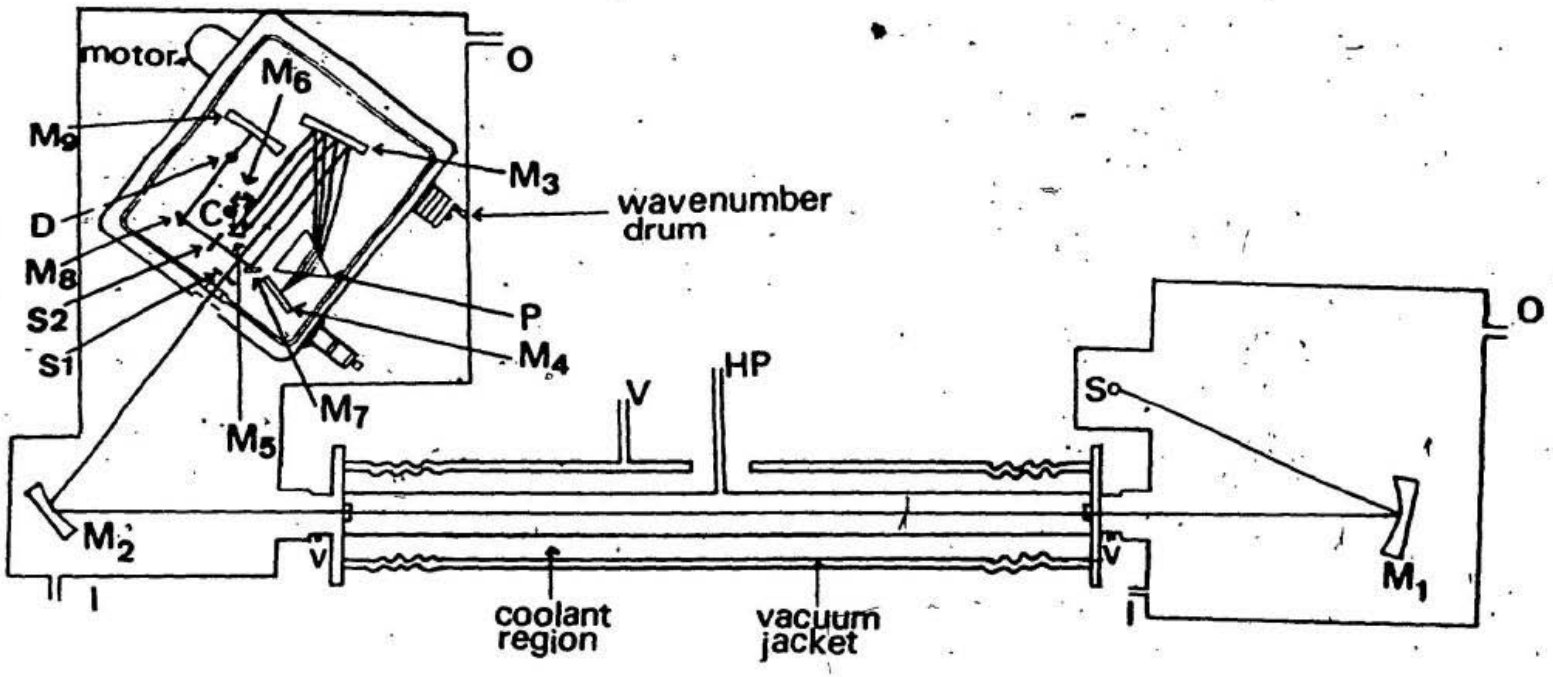

Fig. 3. Arrangement of optics and monochromator in the present experiment. S: source S_1: entrance slit, S_2: exit slit, D: PbS detecor, M_1,M_2 and M_9: spherical mirrors, C: tuning fork chopper, P: prism, M_3: parabolic mirror, M_4: Littrow mirror, M_5-M_8: plane mirrors, I & O: dry nitrogen gas inlet and outlet, respectively, V: to vacuum pump, HP: to high-pressure gas handling system.

2.3 Microprocessor - Controlled DC Stepping Motor

A microprocessor-controlled dc stepping motor (model M091 - FD03, supplied by Superior Electric Company, Connecticut) having a step angle of 1.8° in full step mode and 0.9° in half step mode with a precision of ±5% was used to drive the wavenumber drum. It was operated in a half step mode, and the wavenumber drum was rotated at a step angle of 0.45°, by using an appropriate gear system. A schematic circuit diagram of the stepping motor control unit with appropriate pin connections is shown in Fig. 4(a). An Intel 8255 PPI (to be shown in Fig. 6), controlled by a microcomputer was used to generate the pulses for driving the stepping motor. These pulses were first fed into a Schmitt trigger circuit 74LS14 for pulse shaping and then into the clock input of a 4-bit up/down counter 74LS191. The output of this binary counter was fed into the input of a decimal decoder 74LS42. The output from this decoder was then fed into a 3-input NAND gate 74LS10 and then to a power amplifier circuit as shown in Fig. 4(b). In order to reduce the signal noise, the grounds of the stepping motor and the microcomputer were separated by four optical isolators 4N25, connected between the 74LS10 and power-amplifier circuit (Fig. 4(b)). With the help of the switch shown in Fig. 4(a) the motor can be operated either in a full-step mode or a half-step mode. The up/down input of the 74LS191 counter controls the direction of rotation of the motor.

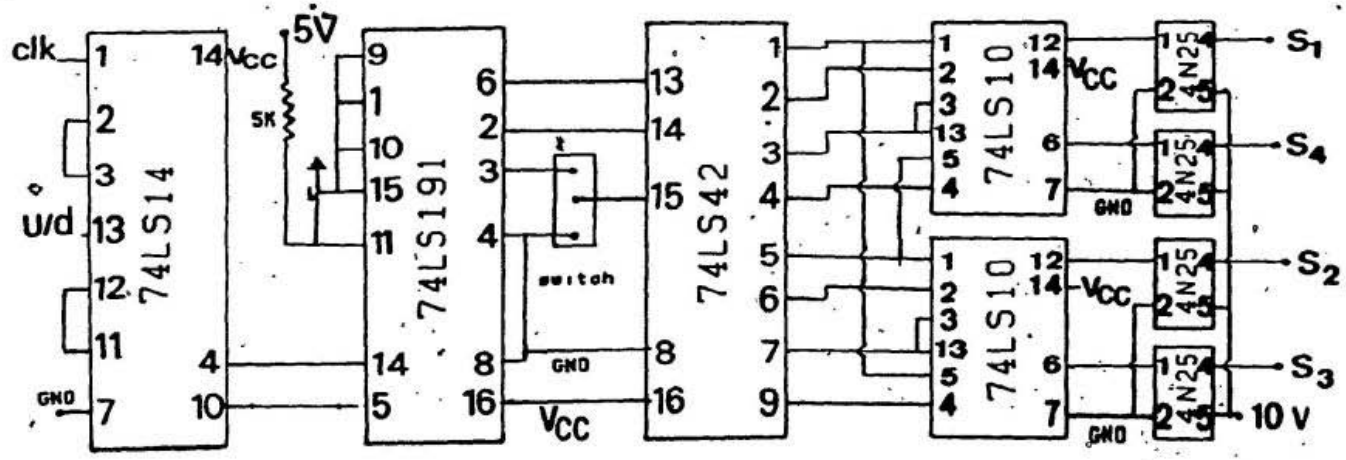

Fig. 4(a) The circuit diagram of the stepping motor control unit. clk: clock input, u/d: up/down input of the counter, GND: ground, V_{cc}: 5 volts, S_1 to S_4 represent the outputs (inputs to the Fig. 4(b)).See also Fig. 4(b).

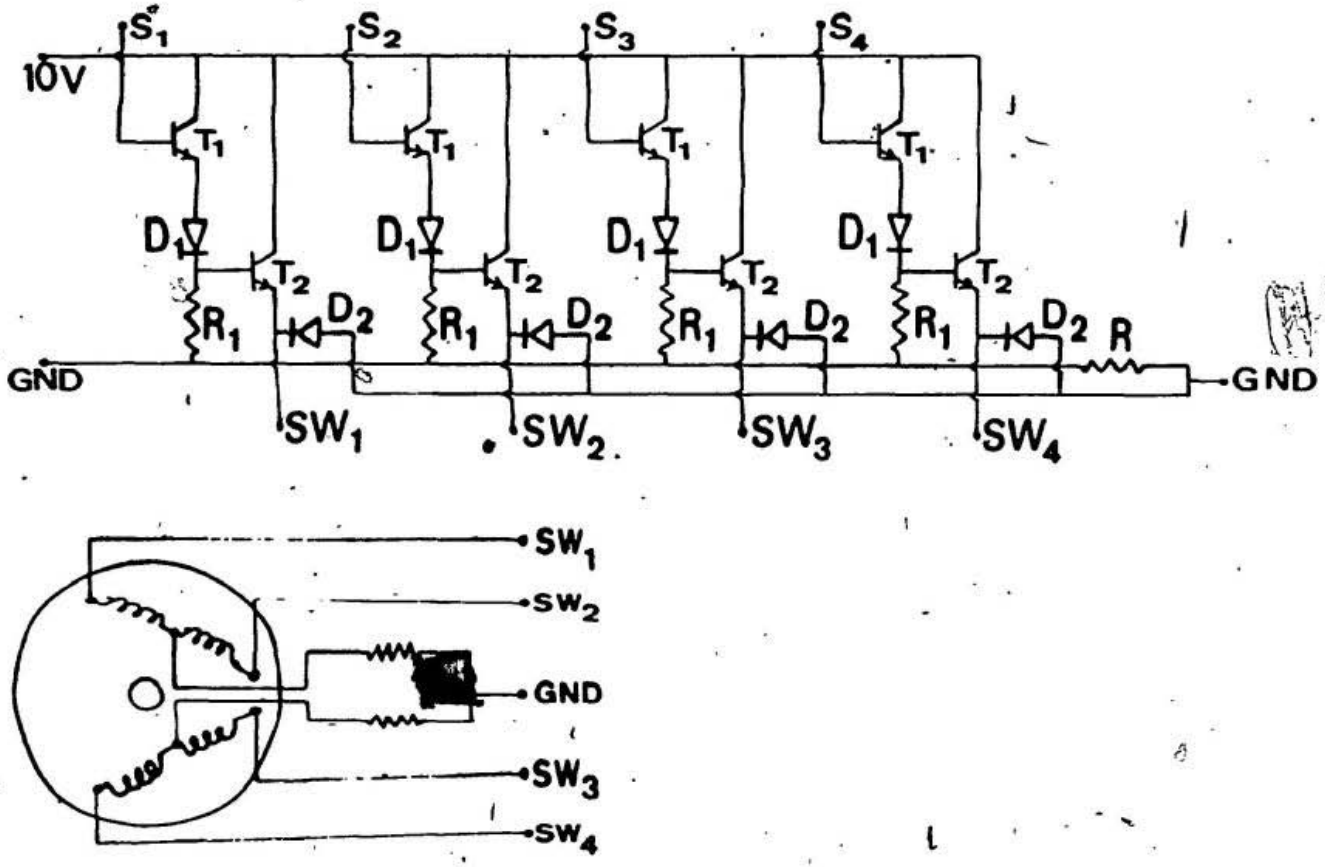

Fig. 4(b)(i) The circuit diagram of the stepping motor control unit. The inputs S_1 to S_4 are from Fig. 4(a). D_1: diode (1N5402), T_1: transistor (ECG123A), T_2: Transistor (2N3055), R: resistor (10 KΩ).

(ii) Connections to the stepping motor.

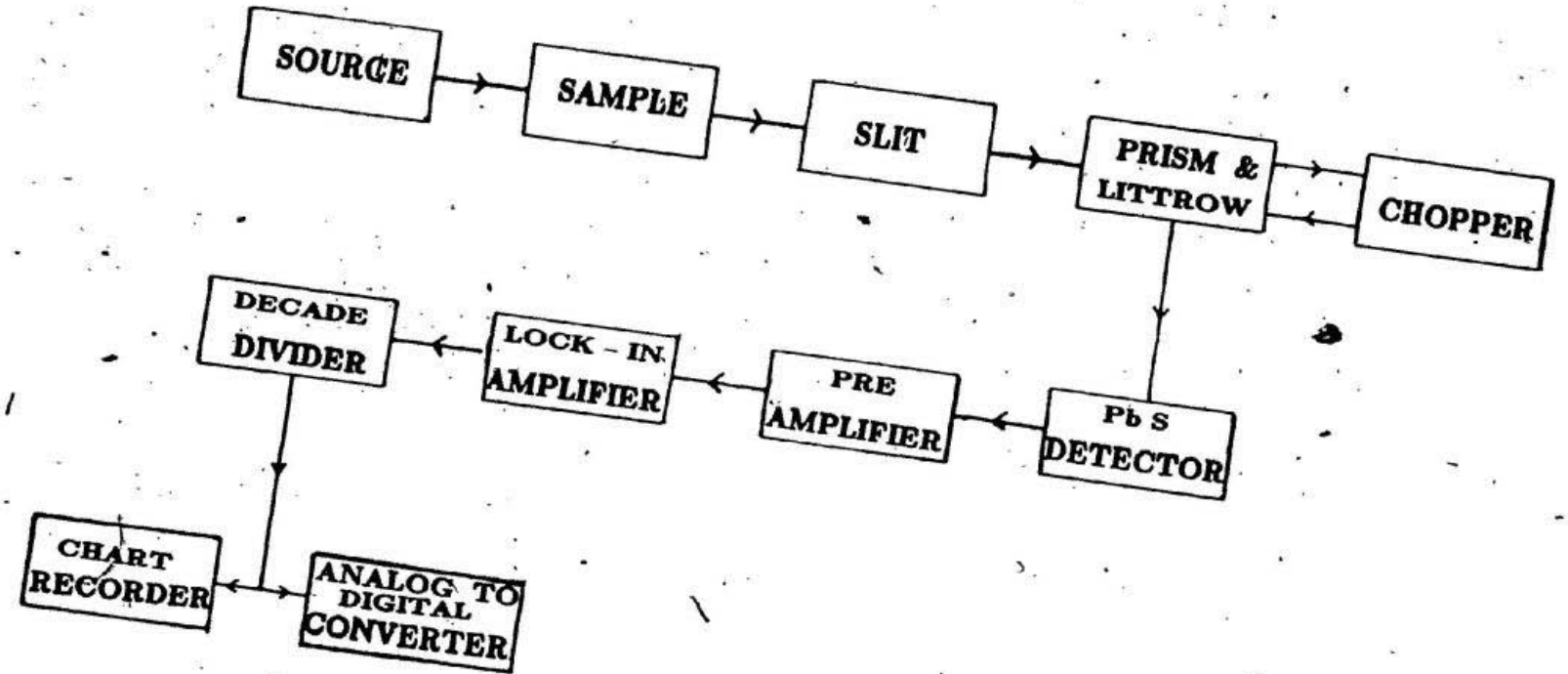

Fig. 5. A block diagram of the signal detection and recording system.

2.4 Detection and Recording of the Signal

A block diagram showing optics and electronics for the signal detection and recording system is shown in Fig. 5. The resistance of a photoconductive device such as a PbS detector used in the present experiment varies with the intensity of radiation falling on it. A constant voltage of 67.5 V was applied to the detector so that the varying resistance of the detector gave rise to a varying voltage signal. This signal was amplified by a Brower Laboratories model 261 preamplifier and model LI-100 lock-in voltmeter. A square wave from the chopper was matched only with the chopped radiation, thus discarding the unchopped first pass radiation. Any ripple in this full wave rectified a.c. signal was filtered out by an RC filter unit. As the acceptable range of the analog-to-digital converter was limited to 0 – 2 volts, an Electro – Measurements Inc., Model DV-412 decade divider was used to attenuate the signal coming from the voltmeter whose range was 0 to 10 volts. This attenuated d.c. signal was then fed to a model 5711 ADC unit controlled by the microprocessor and to a Hewlett Packard model 7132 A strip chart recorder as shown in Fig. 5.

A block diagram of the microprocessor - controlled data acquisition system is shown in Fig. 6. This system was originally designed by Gillard (1983) and was modified in the present work, to accomadate a stepping motor control unit. The microcomputer was based on the Intel 8085 microprocessor and was supplied in kit form by Netronics R & D Ltd. It incorporates a standard S - 100 microcomputer bus and an interpreter for the BASIC language. The Intel 8255 parallel

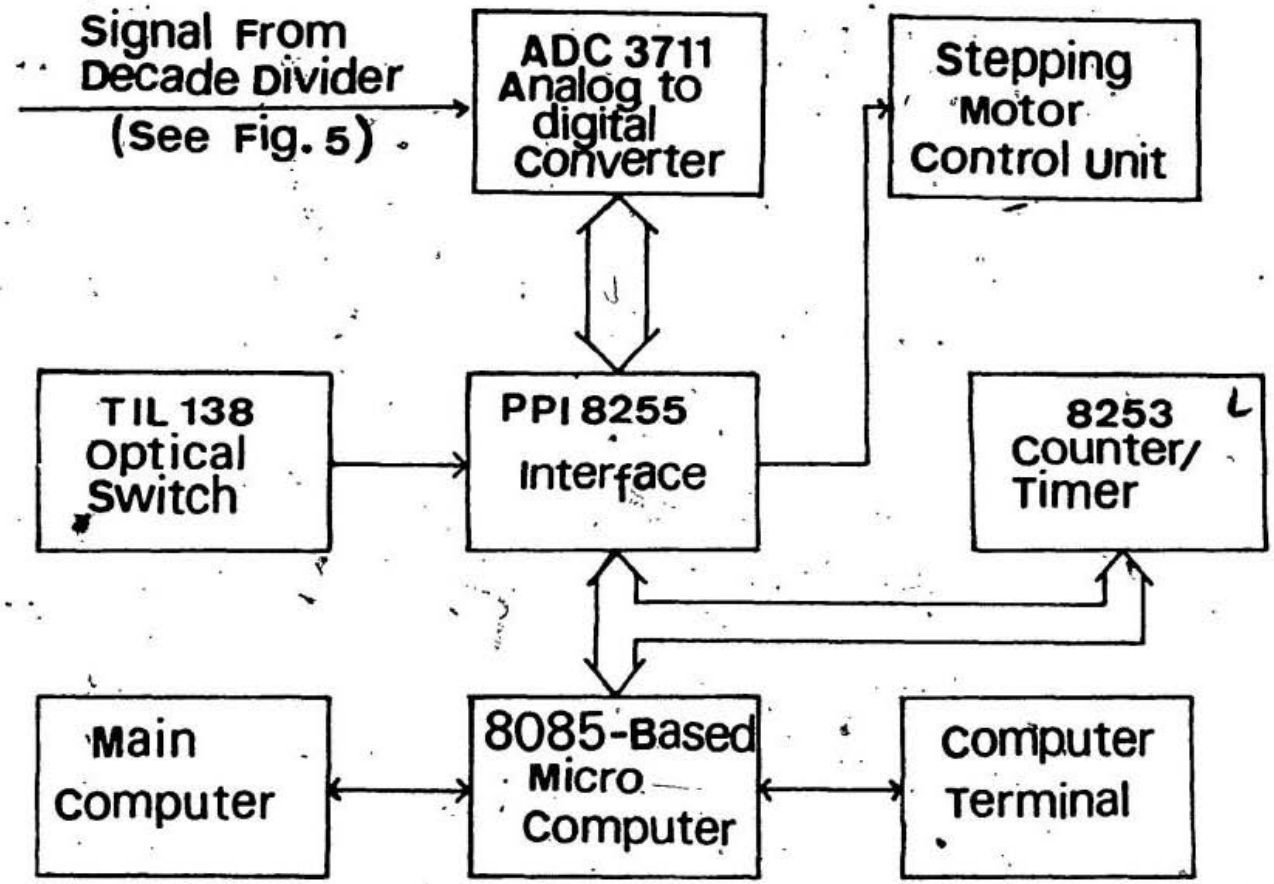

Fig. 6. A block diagram of the microprocessor-controlled data acquisition system.

peripheral interface (PPI) has three individually programmable input/output ports and was used to control the operation of the ADC, stepping motor control unit and the optical switches. The Intel 8253 is a programmable timer chip, which was used to count the number of pulses in a given trace. The ADC converts the lock-in amplifier's output into a decimal number in the range 0 - 4000 for each step. The microcomputer reads the ADC for each step and sends it to the main computer. The optical switches were used to assist the positioning of the wavenumber drum of the monochromator and will be discussed in Section 2.7. For a detailed description of the data-acquistion system, the reader is referred to Gillard (1983).

2.5. The Gas Handling System

The high pressure system used in the present experiments is shown schematically in Fig. 7. Bourdon tube pressure gauges G_1, G_2, and G_3 have the ranges 0 - 20000 p.s.i., 0 - 5000 p.s.i., and 0 - 1000 p.s.i., respectively, and were calibrated against an Ashcroft dead-weight pressure balance having an accuracy of 0.1 %. The Matheson ultra high purity grade hydrogen and argon were used in the present experiments. The hydrogen gas was first passed through a liquid nitrogen trap made of copper tubing, 6.4 mm in outside diameter, before admitting into the absorption cell. A stainless steel thermal compressor was used for developing high pressures of argon. Aminco fittings were used to connect the cell with the gauges, cylinders, traps, and the compressor. The assembled system was tested for pressures up to 15000 p.s.i. and for good vacuum. The base density of

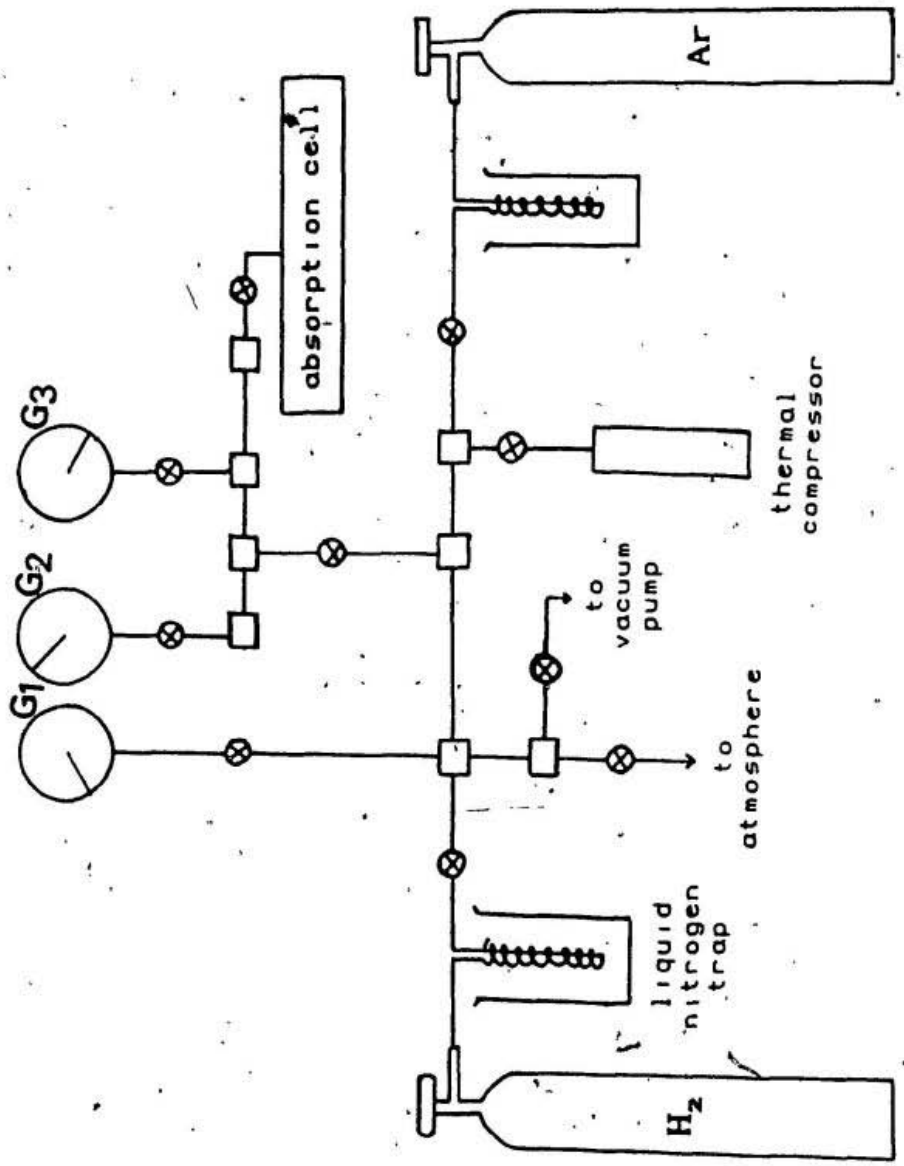

Fig. 7. The high - pressure gas handling system.

hydrogen in the present experiments was in the range 3 - 7 amagat for overlap- and quadrupole- induced transitions and 57 amagat for the hexadecapole-induced transitions. The perturbing gas density was in the range of 15 to 520 amagat.

The argon gas was found to contain small amounts of impurity for pressures greater than 3000 p.s.i., in the spectral region around 5700 cm^{-1}, which was pressure - dependent. For the experiments on the U transitions, the absorption due to impurity was subtracted from the observed absorption profile.

2.6 Isothermal Data of Gases

The gas densities are normally expressed in units of amagat, which is the ratio of the density of a gas at a given temperature and pressure to its density at S.T.P.. The densities of hydrogen were obtained by polynomial least squares fits of the PVT data given by Michels *et al.* (1959). The densities of argon were obtained from Michels *et al.* (1949; 1958), by a similar procedure. The base density ρ_a of hydrogen was directly obtained from its isothermal data.

The partial density ρ_b of the perturbing gas in a binary mixture was determined from the formula (see, for example, Reddy and Cho 1965)

$$\rho_b = \{1/(1 + \beta)\} \{(\rho_a)_p + \beta(\rho_b)_p\} - \rho_a, \qquad (1)$$

where $(\rho_a)_p$ is the density of hydrogen at the total pressure P of the mixture and $(\rho_b)_p$ is the density of the perturbing gas at the same pressure, and $\beta = \rho_b'/\rho_a$ where ρ_b' is the approximate partial density of the perturbing gas corresponding to the partial pressure $P_b = P - P_a$, P_a being the pressure of hydrogen. The

final value of ρ_b was determined by iteration.

2.7 Reduction of Water Vapor from the Optical Path

Absorption due to the atmospheric water vapor in the spectral regions 3500 – 3900 cm^{-1} and 5200 – 5500 cm^{-1} interferes with the recording of the fundamental band of H_2. It was therefore necessary to remove water vapor from the entire optical path from the source of radiation to the detector and this was accomplished in the following manner: The source and mirror M_1 were enclosed in one Plexiglas box (Fig. 3) which was sealed to the end cap of the cell with a rubber tube. The monochromator and mirror M_2 were placed in a second Plexiglas box at the exit end of the cell. Both boxes were fitted with neoprene gloves so that the inside settings could be changed without disturbing the air-tight seal. Dry nitrogen gas developed by passing current through a resistor (100 Ω, 25 W) immersed in a 200 litre liquid nitrogen dewar was passed through the Plexiglas boxes. The outlets of these boxes were fitted with one way valves, to avoid reentry of air into the path of radiation. It took about 4 to 5 days to bring down the water vapor absorption in the system to a negligible and stable level. Flushing with dry nitrogen was continued during the entire experiment.

2.8 Calibration of the Spectral Region and Analysis of the Experimental Data

The spectral region 3500 – 6500 cm^{-1} was calibrated with the standard wave numbers of the mercury emission lines (Humphreys, 1953; Plyer *et al.* 1955; and

Zaidel *et al.* ,1970) and atmospheric water vapor absorption peaks (Downie, 1953; IUPAC Tables of Wavenumbers, 1977).

The spectral region was calibrated by a polynomial least squares fit of the wavenumbers of the standard mercury lines and water vapor absorption peaks against the corresponding pulse numbers of the stepping motor. Once this was done, it was essential to start always at the same point of the wavenumber drum. To ensure the accuracy of the starting point, a Plexiglas circular disc having transparent and opaque markings shown in Fig. 8 was mounted on the wavenumber drum. Two optical switches (TIL 138) were fixed on the body of the monochromator so that the circular disc could be rotated freely, through the air gap of the optical switches. An optical switch consisted of a light-emitting diode (LED) and a phototransistor in a single plastic housing separated by a air gap of 0.318 cm, also shown in Fig. 8. The emitter is connected to the ground of microcomputer and the collector to the PPI (at 5 Volts), through a resistor. When the transparent region of the disc comes in the air gap of the optical switch, light from the LED passes through the circular disc and turns on the phototransistor. Whenever the output of the phototransistor is low, it conducts. On the circular disc a larger opaque mark follows four small opaque marks. The optical switches S_1 and S_2 scan the smaller opaque marks and the larger opaque marks, respectively. The microprocessor reads the optical switches and displays the number 0, 1, 2, or 3 for each step of the motor. The number 0 indicates that both S_1 and S_2 are OFF, 1 indicates S_1 is ON and S_2 is OFF, 2 indicates S_1 is OFF while S_2 is ON, and 3 indicates both S_1 and S_2 are ON.

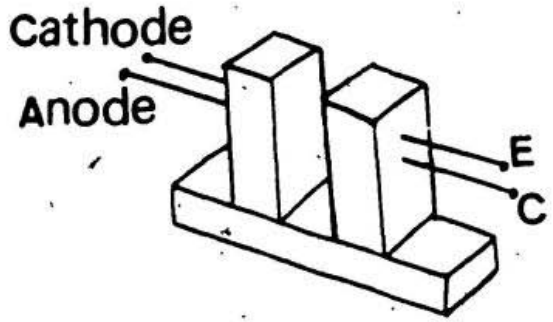

Fig. (a)

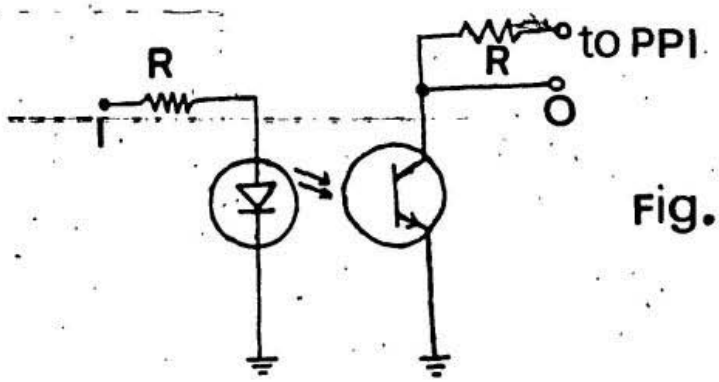

Fig. (b)

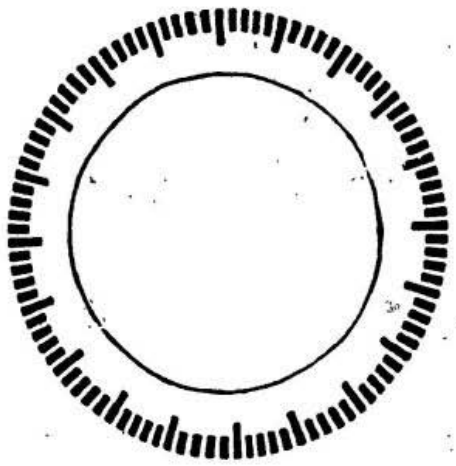

Fig. (c)

Fig. 8. (a) Schematic diagram of an optical switch, E: emitter, C: collector
(b) Circuit diagram of an optical switch, I: input, O: output, R: 200 Ω
(c) Plexiglas disc mounted on the spectrometer.

The enhancement in the absorption coefficient at a given frequency ν (cm^{-1}) due to the addition of a foreign gas into the absorption cell of sample path length l containing a fixed amount of hydrogen gas is given by

$$\alpha_{en}(\nu) = (2.303/l) \log_{10} [I_1(\nu)/I_2(\nu)] , \qquad (2)$$

where $I_1(\nu)$ is the intensity transmitted by the hydrogen gas in the cell and $I_2(\nu)$ is the intensity transmitted by the binary gas mixture. The quantity $\log_{10} [I_1(\nu)/I_2(\nu)]$ was measured for each pulse number, with the aid of a computer program. Absorption profiles were then obtained by plotting $\log_{10} [I_1(\nu)/I_2(\nu)]$ against wavenumber (ν). The integrated absorption coefficient $\int \alpha_{en}(\nu)\, d\nu$ was obtained from the areas under the absorption profiles.

CHAPTER 3

ENHANCEMENT ABSORPTION PROFILES AND ABSORPTION COEFFICIENTS

A brief outline of the previous work on the collision-induced absorption of the fundamental band of gaseous H_2 and the objectives of the present research project are given in Chapter 1. Details of the experimental apparatus and techniques are described in Chapter 2. The collision-induced fundamental band of H_2 in H_2 - Ar mixtures has been studied at 201, 273, and 296 K with a 2 m absorption cell for several base densities of H_2 and argon densities up to 160 amagat at 201 and 273 K and up to 520 amagat at 296 K. In the present chapter the enhancement absorption profiles of the band for gas densities up to 160 amagat, consisting of mainly the overlap and quadrupole- induced transitions, will be presented along with the derived absorption coefficients. Table I summarizes the conditions under which the experimental profiles presented in this chapter were obtained.

TABLE I

Summary of the experimental conditions

Temperature (K)	Sample path length (cm)	Maximum density of the perturbing gas (amagat)	Number of mixture densities studied
201	185.9	126	25
273	186.0	158	35
296	186.1	152	28

3.1 Enhancement Absorption Profiles

Figures 9, 10, and 11 show three typical sets of the experimental enhancement absorption profiles of the fundamental band of H_2 in the spectral region 3800 – 5300 cm^{-1} in the binary mixtures of H_2 – Ar at 201, 273 and 296 K, respectively. In each of these figures the quantity $\log_{10} [I_1(\nu)/I_2(\nu)]$ is plotted against wavenumber ν (in. cm^{-1}) for a fixed base density of H_2 and three different densities of the argon gas. The positions of the collision-induced single transitions $O_1(2)$, $Q_1(J)$, and $S_1(J)$ for $J = 0$ to 3, calculated from the constants of the free H_2 molecule (Stoicheff 1957) are marked along the wavenumber axis.

In all the profiles, the main dip of the Q-branch occurs at the position of $Q_1(1)$ line (4155 cm^{-1}). This dip was explained by Van Kranendonk (1968) (see also Lewis, 1985 and the references therein) as a result of destructive interference occurring between the overlap dipole moments in successive collisions. The two peaks at the low- and high-wavenumber sides of this dip are designated by Q_P and Q_R respectively and the separation $\Delta\nu_{PR}^{max}$ between them increases with the density of the perturbing gas. The widths of the individual components in collision-induced spectra have a characteristic dependence on the temperature. At higher temperatures, because of the larger relative translational energy of the colliding molecules, the collision duration is small and the widths are relatively broad. At lower temperatures, the components are relatively narrow.

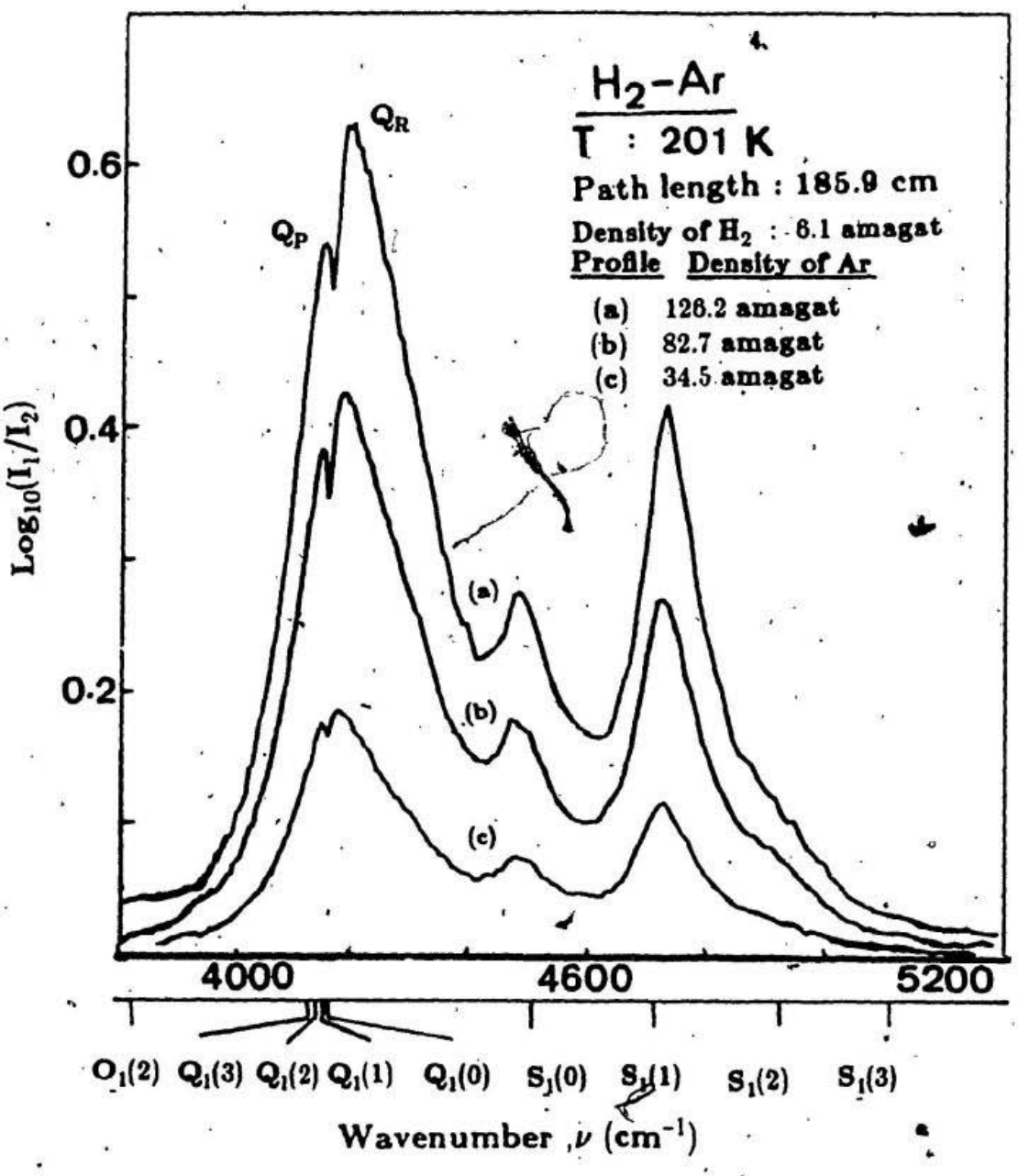

Fig. 9. The enhancement absorption profiles of the fundamental band of H_2 in three mixtures of H_2-Ar at 201 K.

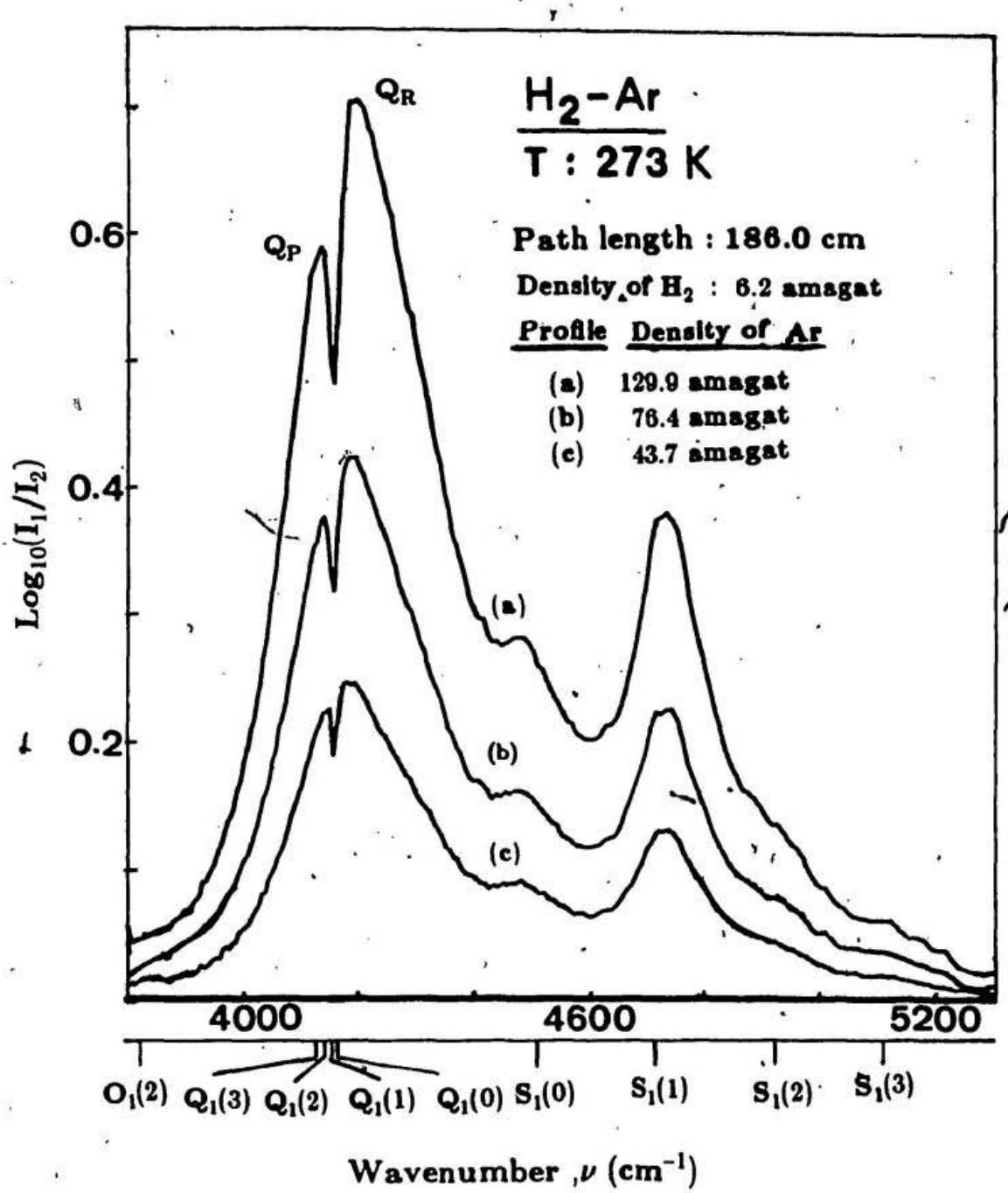

Fig. 10. The enhancement absorption profiles of the fundamental band of H_2 in three mixtures of H_2-Ar at 273 K.

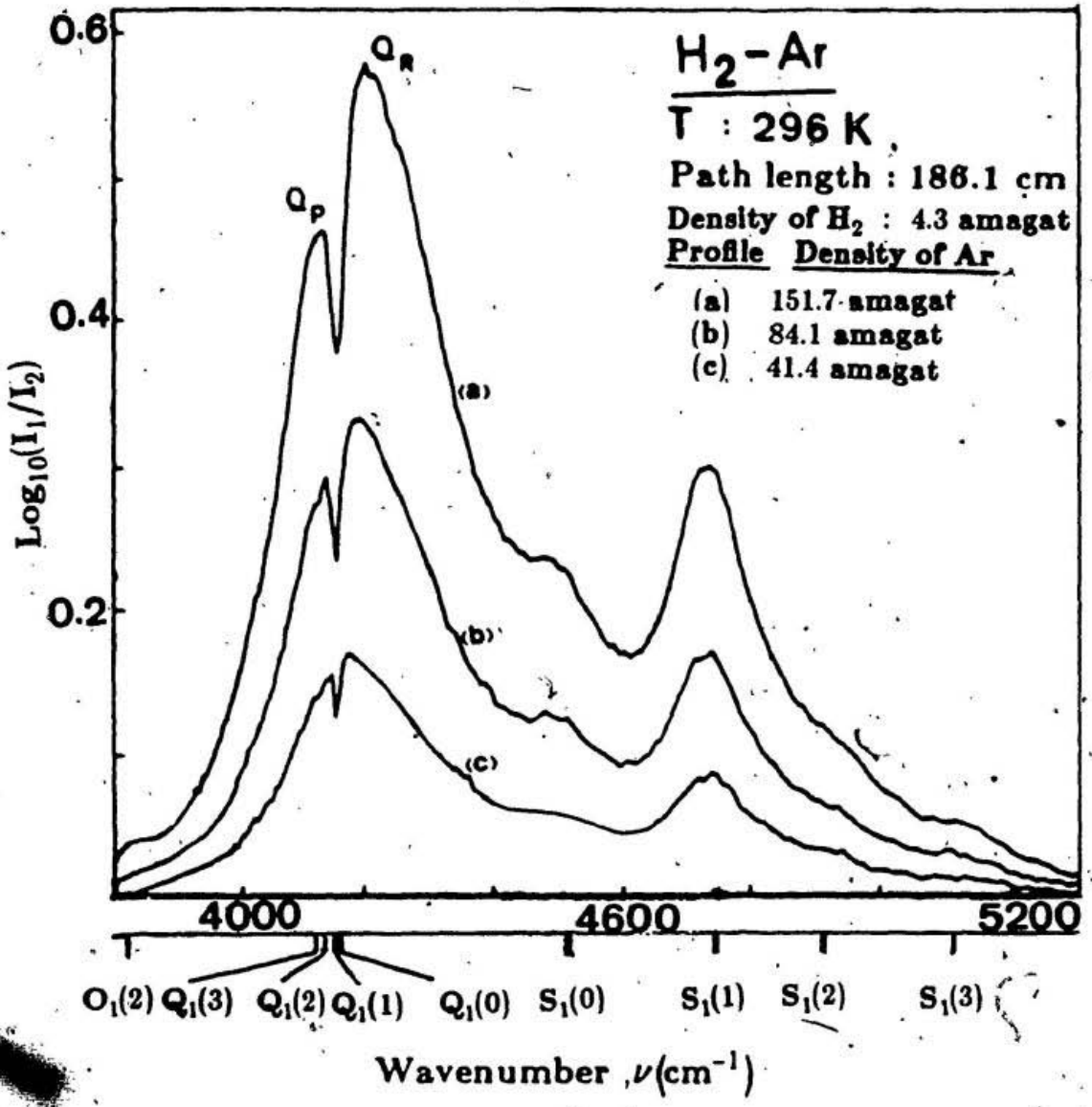

Fig. 11. The enhancement absorption profiles of the fundamental band of H_2 in three mixtures of H_2-Ar at 296 K.

3.2 Absorption Coefficients

The enhancement of the integrated absorption coefficient of a band depends on the partial densities ρ_a ($=\rho_{H_2}$) and ρ_b ($=\rho_{Ar}$) and is expressed by the relation

$$\int \alpha_{en}(\nu)\, d\nu = \alpha_{1b}\, \rho_a\, \rho_b + \alpha_{2b}\, \rho_a\, \rho_b^2 + \cdots$$

or

$$(1/\rho_a\rho_b) \int \alpha_{en}(\nu)\, d\nu = \alpha_{1b} + \alpha_{2b}\, \rho_b + \cdots, \qquad (3)$$

where α_{1b} (cm^{-2} $amagat^{-2}$) and α_{2b} (cm^{-2} $amagat^{-3}$) are the binary and ternary coefficients, respectively. The values of $(1/\rho_a\rho_b) \int \alpha_{en}(\nu)\, d\nu$ for H_2 - Ar at three different temperatures, 201, 273, and 296 K, are plotted in Fig. 12. The plots are found to be straight lines in all the three cases. The intercepts and slopes of these plots were obtained by linear least square fits of the experimental data. The binary and ternary absorption coefficients, which are represented by the intercepts and slopes , respectively, are listed in Table II. It can be seen from Table II that the binary absorption coefficients are very large compared to the ternary coefficients, indicating that the main contribution to the collision- induced absorption comes from the binary collisions.

In order to compare with theory, the enhancements of the integrated absorption coefficient can also be expressed as

$$c \int \tilde{\alpha}_{en}(\nu)\, d\nu = \tilde{\alpha}_{1b}\, \tilde{\rho}_a\, \tilde{\rho}_b + \tilde{\alpha}_{2b}\, \tilde{\rho}_a\, \tilde{\rho}_b^2 + \cdots, \qquad (4)$$

where c is the speed of light, $\tilde{\alpha}_{en}(\nu) = \alpha_{en}(\nu)/\nu$ is the enhancement in the absorption coefficient with the frequency factor removed, and $\tilde{\rho}_a$ and $\tilde{\rho}_b$ are the number

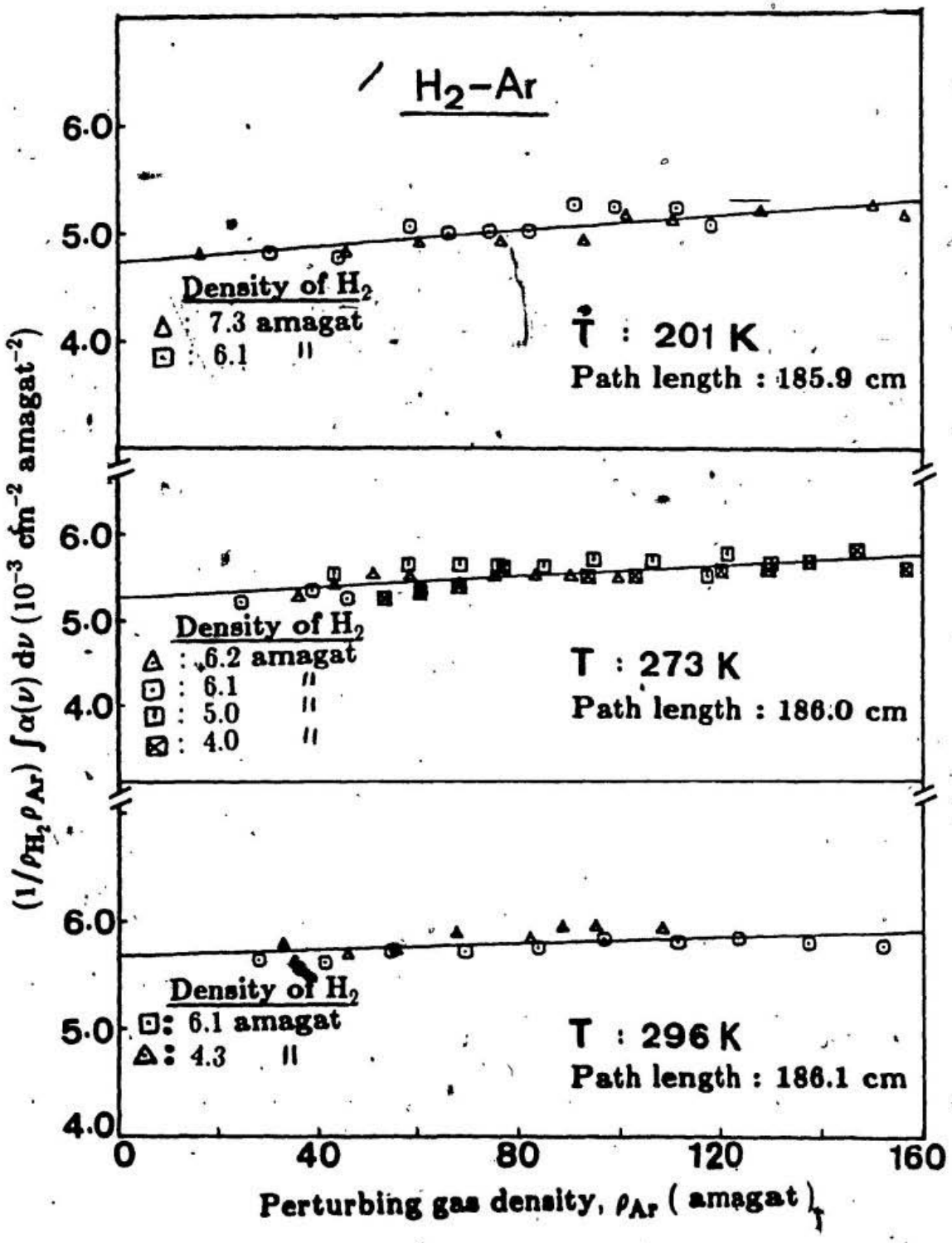

Fig. 12. Plots of $(1/\rho_a\rho_b)\int\alpha(\nu)d\nu$ vs. ρ_b for the enhancement absorption profiles.

TABLE II.

Absorption coefficients[a] of the fundamental band of H_2-Ar binary mixture at 201, 273 and 296K.

Temperature T (K)	Binary absorption coefficient α_{1b} (10^{-3} cm^{-2} $amagat^{-2}$)	α_{1b} (10^{-35} cm^6 s^{-1})	Ternary absorption coefficient α_{2b} (10^{-6} cm^{-2} $amagat^{-3}$)
201	4.73 ± 0.05	4.48 ± 0.05	4.87 ± 0.77
273	5.27 ± 0.05	4.99 ± 0.05	3.03 ± 0.55
296	5.68 ± 0.05[b]	5.37 ± 0.05	1.44 ± 0.61

a Ranges of error indicated are standard deviations.

b The binary coefficient at 298 K quoted by Prasad (1976) is 5.99 + 0.06.

densities (number of molecules per unit volume) of the absorbing and perturbing gases, respectively. These densities are related to those expressed in amagat units

$$\tilde{\rho}_a = \rho_a \, \eta_0 ; \quad \tilde{\rho}_b = \rho_b \, \eta_0, \tag{5}$$

where η_0 is Loschmidt's number (number density of an ideal gas at S.T.P., 2.687 x 10^{19} cm^{-3}). The new binary and ternary absorption coefficients are related to the previous ones by the relations

$$\tilde{\alpha}_{1b} = (c/\eta_0^2) \, \alpha_{1b}/\bar{\nu} , \quad \tilde{\alpha}_{2b} = (c/\eta_0^3) \, \alpha_{2b}/\bar{\nu}, \tag{6}$$

where the band center $\bar{\nu}$ is given by

$$\bar{\nu} = \int \alpha_{en}(\nu) \, d\nu / \int \nu^{-1} \, \alpha_{en}(\nu) \, d\nu. \tag{7}$$

The average values of $\bar{\nu}$ at 201, 273, and 296 K are 4381, 4385 and 4390 cm^{-1}, respectively. The values of $\tilde{\alpha}_{1b}$ are also listed in the Table II. Even though, extreme care was taken in recording the absorption profiles, small errors due to uncertainities from the spectral region calibration (standard deviation is 0.3 cm^{-1}), ADC system (non-linearity is ±0.025% of full scale or 1 count), area calculations of the absorption profiles (the trapezoidal rule used in the area calculation gives the good approximation only), noise etc. could be present in this data. The contribution of these errors to the presented data is very small and lies with in the experimental accuracy.

CHAPTER 4

ANALYSIS OF THE ENHANCEMENT ABSORPTION PROFILES

As discussed in Chapter 1, the absorption profiles presented in Chapter 2 occur mainly as a result of a short-range electron-overlap interaction and a long-range quadrupolar interaction. The quantity μ_{ov} which arises due to the distortion of the electron charge distribution of the colliding pairs of molecules gives rise to the $Q_{ov}(J)$ transitions. On the other hand, μ_q, which results from the polarization of a molecule (e.g. Ar) by the quadrupole field of its collision partner (e.g. H_2), gives rise to various single transitions in the O, Q, and S branches. In this chapter, the contributions of the individual transitions to the total enhancement of absorption of the band will be separated by a method of profile analysis and the characteristic half-width parameters of the overlap- and quadrupole-induced components will be obtained for the observed absorption profiles.

4.1 Line Shape Functions

It is convenient to express the dimensionless absorption coefficient $\tilde{\alpha}_{en}(\nu)$ $(= \alpha_{en}(\nu)/\nu)$ at a given wavenumber ν by the relation (Van Kranendonk, 1968; Mactaggart and Welsh, 1973)

$$\tilde{\alpha}_{en}(\nu) = \sum_{m,n} \frac{\tilde{\alpha}^0_{nm}\, W_n(\Delta\nu)}{1 + \exp(-h\,c\,\Delta\nu / k\,T)}, \qquad (8)$$

where n stands for the induction mechanism (n = ov for the overlap induction and n = q for the quadrupole induction), m represents a specific transition arising from a given mechanism, $\tilde{\alpha}^0_{nm}$ is a parameter indicating the maximum absorption coefficient at the molecular frequency ν_m (cm^{-1}), $W_n(\Delta\nu)$ with $\Delta\nu = \nu - \nu_m$ represents the line shape function of the n-type of mechanism, h, c, and k are the fundamental constants, and T is the absolute temperature. All the spectral transitions arising from a given induction mechanism can be represented by the same line shape function (Poll, 1961). The factor $[1 + \exp(-h\,c\,\Delta\nu/k\,T]$ on the right side of Eq. (8) converts the symmetrized line shape $\tilde{\alpha}^0_{nm}\,W_n(\Delta\nu)$ into the observed asymmetric line shape and this satisfies the so-called "detailed balance condition" (see, for example, Reddy, 1985).

The line shape function $W_{ov}(\Delta\nu)$ of an overlap- induced transition in Eq. (8) can be expressed (Van Kranendonk, 1968) as

$$W_{ov}(\Delta\nu) = W^0_{ov}(\Delta\nu)\,D(\Delta\nu)\,, \qquad (9)$$

where $W^0_{ov}(\Delta\nu)$ is the intracollisional line form arising from the single binary collisions and $D(\Delta\nu)$ is the intercollisional line form, which takes into account the correlation existing between the dipole moments induced in successive collisions. The quantity W^0_{ov} is represented by the Levine-Birnbaum (1967) expression as

$$W^0_{ov}(\Delta\nu) = (2\,\Delta\nu/\delta_d)^2\,k_2(2\Delta\nu/\delta_d)\,, \qquad (10)$$

Where k_2 is the modified Bessel function of the second kind and δ_d is the intracollisional half-width at half-height. The function $D(\Delta\nu)$ as represented by Van

Kranendonk (1968) (see also Lewis, 1976) is

$$D(\Delta\nu) = 1 - \gamma\,[1 + (\Delta\nu/\delta_c)^2]^{-1}\,, \qquad (11)$$

where γ is a constant (which is assumed to be unity in the present analysis), and δ_c is the intercollisional half-width at half-height. The line shape functions for an overlap-induced component are represented schematically in Fig. 13.

The line shape function $W_q(\Delta\nu)$ of a quadrupole-induced transition in Eq. (8) is normally represented by a dispersion-type (i.e., Lorentz-type) line shape function (which is symmetric about ν_m) and is expressed as

$$W_q(\Delta\nu) = 1/[1 + (\Delta\nu/\delta_q)^2]\,, \qquad (12)$$

where δ_q is the quadrupolar half-width at half-height. However, at the high-wavenumber tail of the fundamental band, the simple dispersion line shape represented by Eq. (12) is not entirely satisfactory, particularly for the profiles obtained at high densities. Reddy *et al.* , (1980) and Gillard *et al.* (1984)) included a $(\Delta\nu/\delta_{q_4})^4$ term in the denominator of the dispersion-type function to obtain a satisfactory fit. The modified dispersion line shape function is represented by

$$W'_q(\Delta\nu) = 1/[1 + (\Delta\nu/\delta_{q_2})^2 + (\Delta\nu/\delta_{q_4})^4]\,. \qquad (13)$$

Lewis and Tjon (1978) have shown that $(\Delta\nu/\delta_{q_4})^4$ in the denominator of a Lorentz line shape (Eq. 12) is the dominant asymptotic term for a hard repulsive force, This term, although not exact, should give a good approximation for the quadrupole-induced lines because the length scale of the induced dipole moment

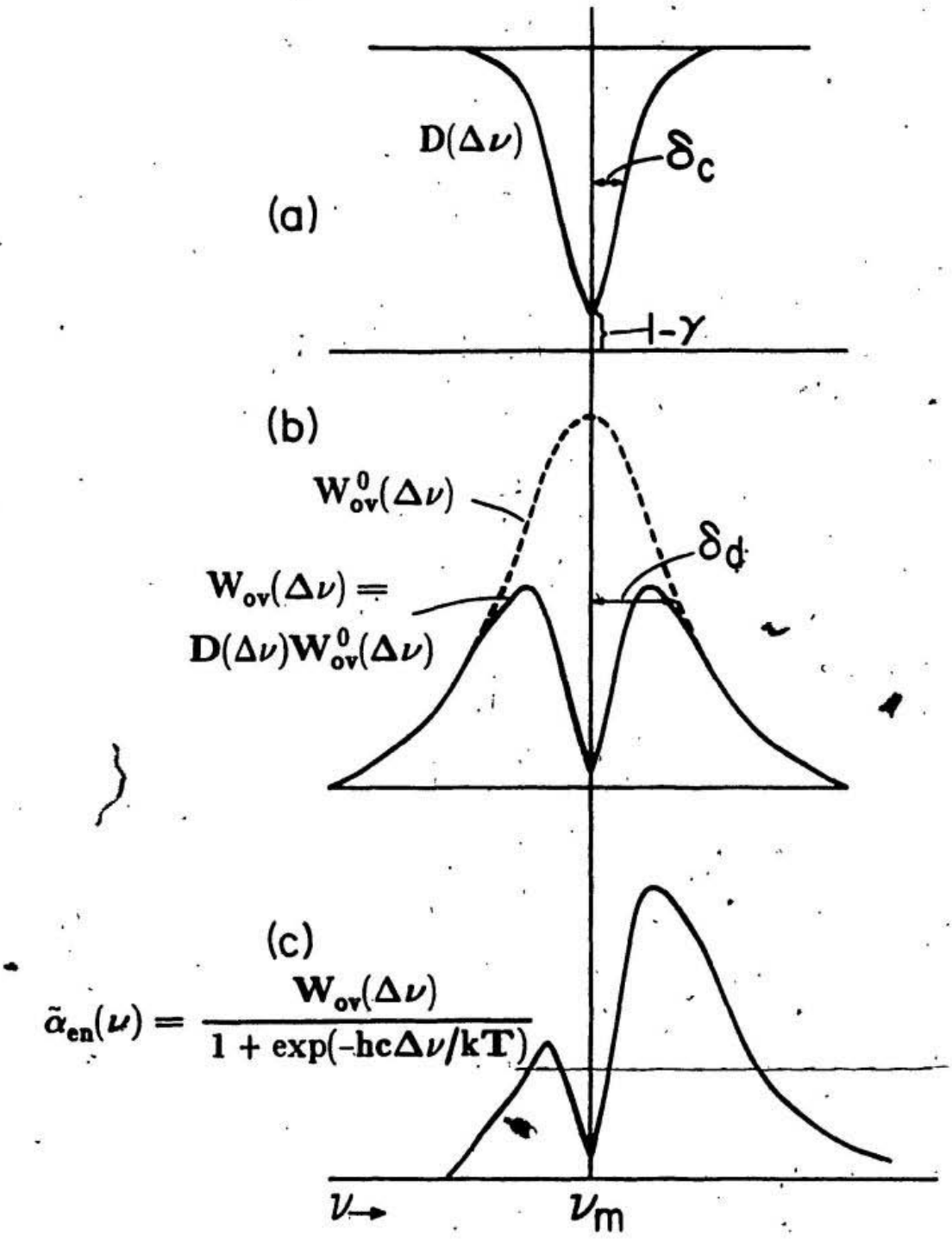

Fig. 13. Line shape for an overlap - induced component:
(a) Intercollisional line form, $D(\Delta\nu)$.
(b) Dashed curve represnts intracollisional line form, W^0_{ov}. Solid curve represents the product of above two line forms
(c) The observed line form obtained by dividing $W_{ov}(\Delta\nu)$ with $[1+\exp(-hc\Delta\nu/kT)]$.

$\mu_q(R)$ is greater than the length scale in which the radial motion of the colliding molecules reverses. The quadrupolar line shapes (Eqs. (12) and (13)) are illustrated in Fig. 14.

4.2 Relative Intensities

The relative intensity of an overlap-induced transition, m, is represented by (Van Kranendonk, 1958)

$$\tilde{\alpha}_{ov\,m} \propto P_J , \tag{14}$$

where P_J is the normalized Boltzmann factor for the rotational state J (note: $\sum_J P_J = 1$) and is given by

$$P_J = \frac{g_T (2J + 1) \exp(-E_J/kT)}{\sum_J g_T (2J + 1) \exp(-E_J/kT)} . \tag{15}$$

Here, g_T is the nuclear statistical weight factor (it is 1 for even J and 3 for odd J for H_2), and E_J is the energy of the rotational level J. Equation (15) is true for equilibrium hydrogen. For normal hydrogen, $\sum_{J,odd} P_J / \sum_{J,even} P_J = 3/1$. The relative intensities of the overlap transitions were expressed in terms of the intensity of the strongest line $Q_{1\,ov}(1)$ and are presented in Table III.

The integrated binary absorption coefficient of a specific quadrupole-induced transition m in H_2 - Ar arising from the isotropic polarizability of argon is given by (Poll, 1971; Karl *et al.* ,1975; see also Reddy, 1985)

$$\tilde{\alpha}_{qm} = (4\pi^3 e^2/3hc)\, n_0^2\, a_0^5 (a_0/\sigma)^5\, J_q\, X_{qm} , \tag{16}$$

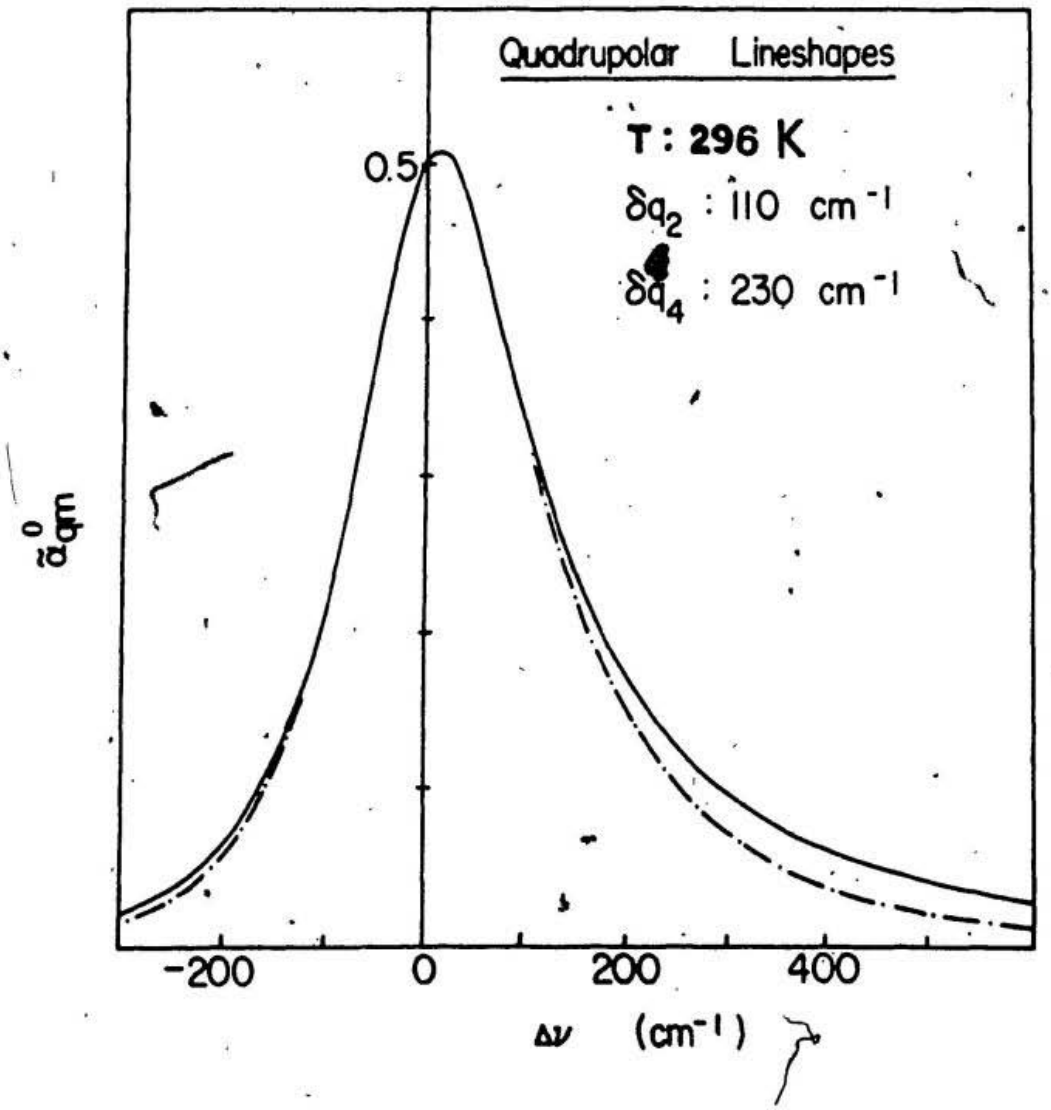

Fig. 14. Line shape for a quadrupole - induced component. The solid line represents the observed line shape with δ_q=110 cm^{-1}. While the dash-dot line represents the lineshape with the δ_{q2}=110 cm^{-1} and δ_{q4}=230 cm^{-1} at 296 K.

TABLE III

Relative intensities of the overlap and quadrupolar transitions of the fundamental band of H_2

Transition	Wavenumber (cm^{-1})	Relative intensity 201 K	273 K	296 K
	Overlap transitions			
$Q_{ov}(3)$	4125.8	0.035	0.106	0.135
$Q_{ov}(2)$	4143.4	0.098	0.161	0.178
$Q_{ov}(1)$	4155.2	1.000	1.000	1.000
$Q_{ov}(0)$	4161.1	0.247	0.208	0.200
	Quadrupolar transitions			
$O_1(3)$	3568.2	0.040	0.096	0.120
$O_1(2)$	3806.7	0.073	0.098	0.109
$Q_1(3)$	4125.8	0.023	0.071	0.090
$Q_1(2)$	4143.4	0.070	0.114	0.127
$Q_1(1)$	4155.2	0.993	0.993	0.993
$S_1(0)$	4497.8	0.487	0.410	0.394
$S_1(1)$	4712.9	1.000	1.000	1.000
$S_1(2)$	4917.2	0.070	0.115	0.128
$S_1(3)$	5109.0	0.019	0.058	0.073

where

$$X_{qm} = P_J\, C(J\,2J';\,00)^2\, <0J \mid Q \mid 1J'>^2 \alpha_{Ar}^2 \quad . \qquad (17)$$

In Eq. (16), $J_q(T)$ is a temperature-dependent dimensionless integral for the quadrupolar induction, a_0 is the Bohr radius, σ is the molecular diameter of the colliding pair corresponding to zero intermolecular potential. At a given temperature, all the terms except X_{qm} in Eq. (16) are common for all the transitions. In Eq. (17), α_{Ar} is the polarizability of the argon molecule, P_J is the normalized Boltzmann factor for the H_2 molecule, $C\,(J\,2J';\,00)$ are Clebsch-Gordan coefficients (Rose, 1957), $<0J \mid Q \mid 1J'>$ are the quadrupolar matrix elements of H_2 taken from Hunt *et al.* , 1984. The relative intensities of the quadrupolar transitions expressed in terms of the intensity of the strongest line $S_1(1)$ are presented in Table III.

4.3 Computational Procedure

In order to separate the overlap and quadrupolar contributions to the total enhancement absorption of the band, a non-linear least squares fit program written by Gillard (1983) in FORTRAN was used. This program requires two absorption maxima parameters $\tilde{\alpha}^{o}_{ov\,m}$ and $\tilde{\alpha}^{o}_{q\,m}$ for the overlap and quadrupolar components, respectively, and three (or four) half-width parameters δ_c, δ_d, and δ_q (or δ_{q_1} and δ_{q_2}) defined by Eqs. (10) to (13). By adjusting these parameters, computation was performed until the computed profile which was the sum of all the individual components gave the best non-linear least squares fit to

the experimental profile over the entire region of the band. The analysis of a typical profile at 273 K for a H_2 – Ar mixture is shown in Fig. 15. In this fit Eq. (13) was used for the quadrupolar lines. In Fig. 15 the individual overlap and quadrupolar components are shown by dashed lines. The overlap components can be easily distinguished by their characteristic dips. Examples of the profile analysis at 296 K are shown in Figs. 16 and 17, and the analysis of a profile at 201 K is shown in Fig. 18. In Figs. 17 and 18, only the total overlap and quadrupolar contributions to the experimental profiles are shown along with the synthetic profiles.

4.4 Result of Profile Analysis

Profile analysis of the enhancement of absorption was carried out for all the experimental profiles using the procedure outlined in Sec. 4.3, and the results of the analysis are presented in Table IV. The overlap contribution to the total enhancement of absorption decreases from 43% at 201 K to 40% at 296 K, and the quadrupolar contribution increases from 57% at 201 K to 60% at 296 K. The collision duration τ_d and τ_q, calculated from the relations

$$\tau_d = 1/2\pi c\delta_d \quad \text{and} \quad \tau_q = 1/2\pi c\delta_q, \qquad (18)$$

are also listed in Table IV. The half-widths δ_d and δ_q, for each of the mixtures remain constant at a given temperature within the range of gas densities studied; however, the intercollisional half-width δ_c increases with density. This increase can be understood from the fact that as the density of gas mixture increases, the

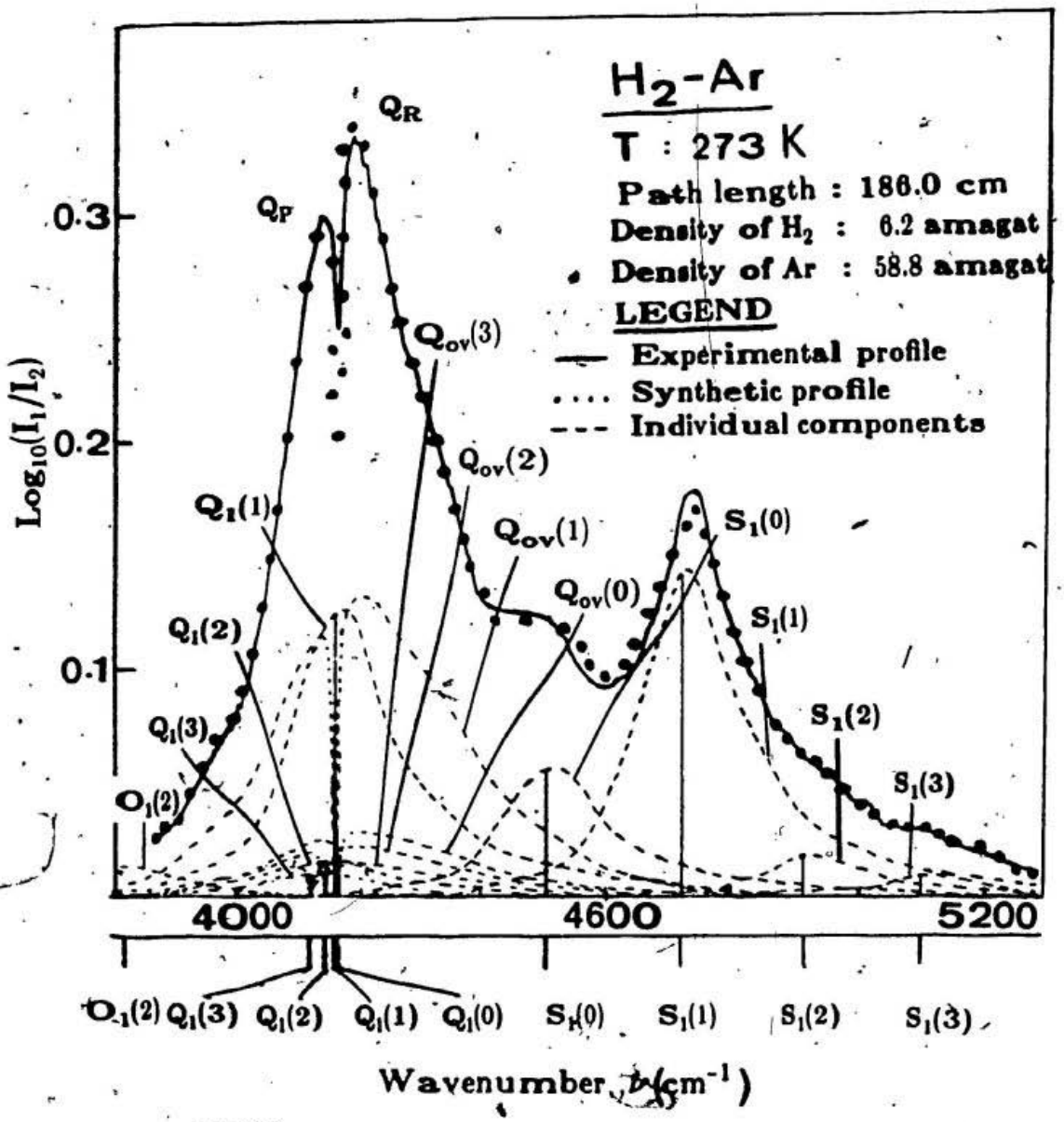

Fig. 15. Analysis of an enhancement absorption profile obtained in a H_2 - Ar mixture at 273 K. All the quadrupolar components are marked along the wavenumber axis. The relative intensities of the quadrupolar components are shown by the stick spectra.

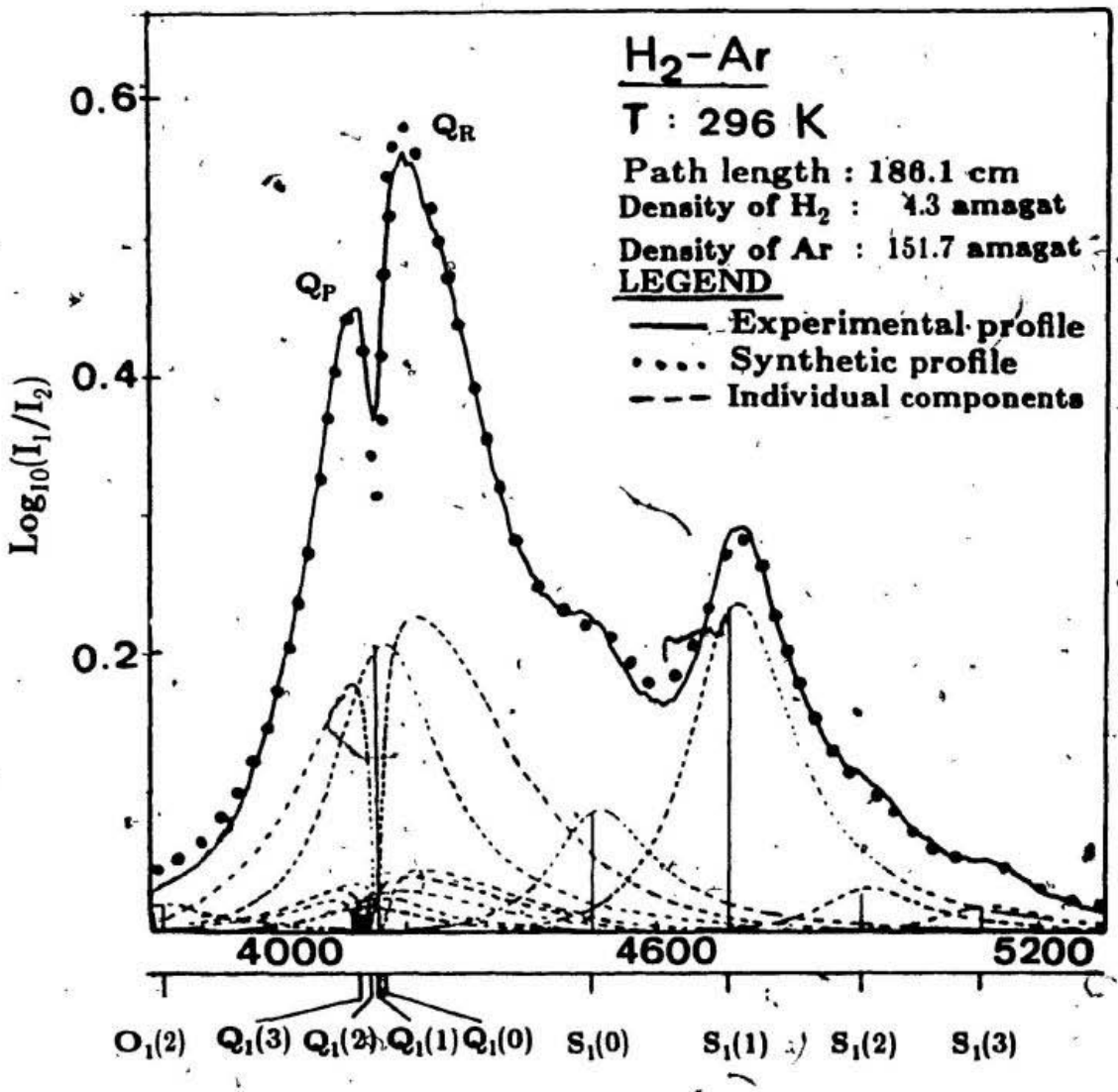

Fig. 16. Analysis of an enhancement absorption profile obtained in a H_2-Ar mixture at 296 K. All the quadrupolar components are marked along the wavenumber axis. The relative intensities of the quadrupolar lines are shown by the stick spectra.

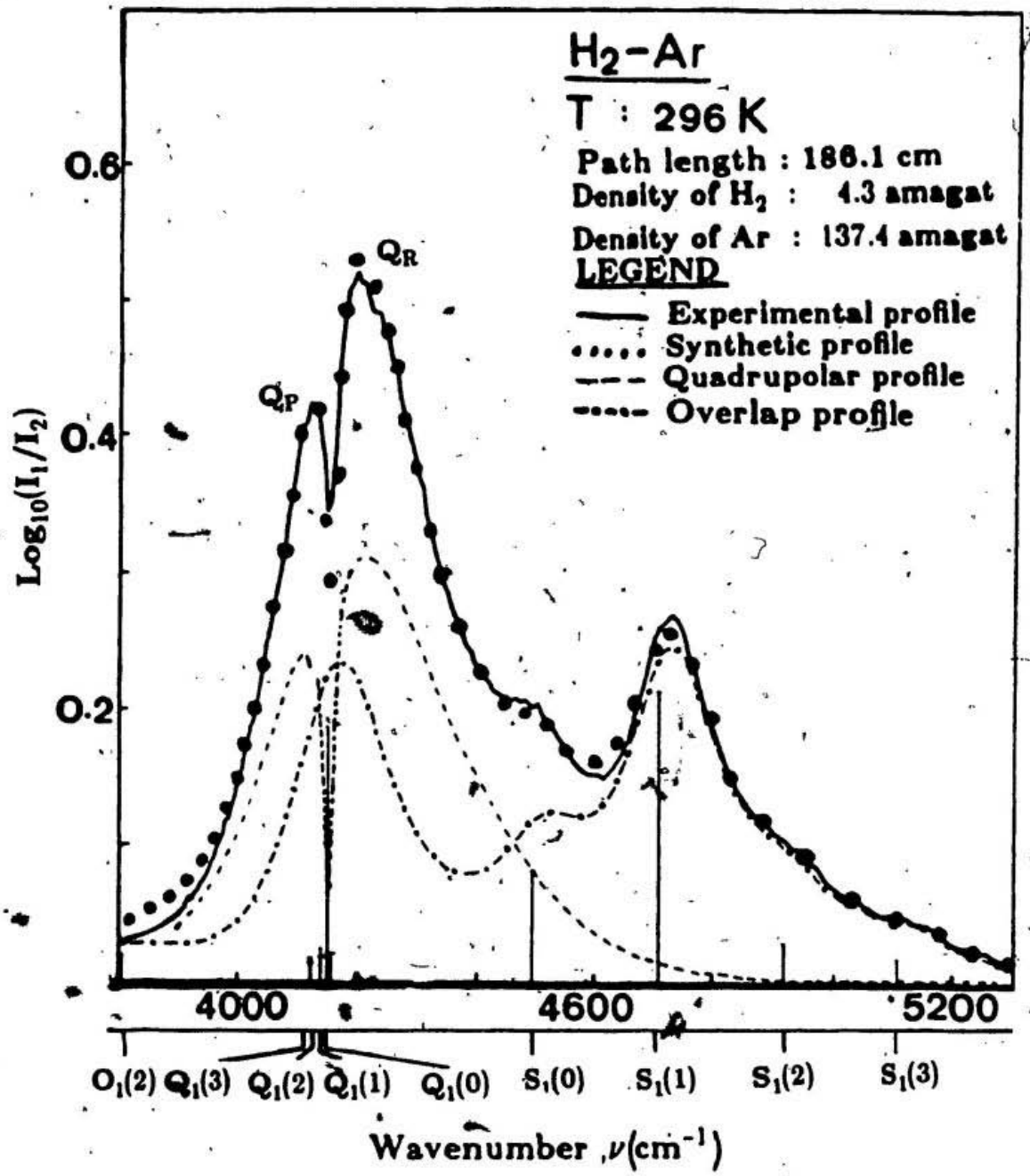

Fig. 17. Analysis of an enhancement absorption profile obtained in a H_2 - Ar binary mixture at 296 K.

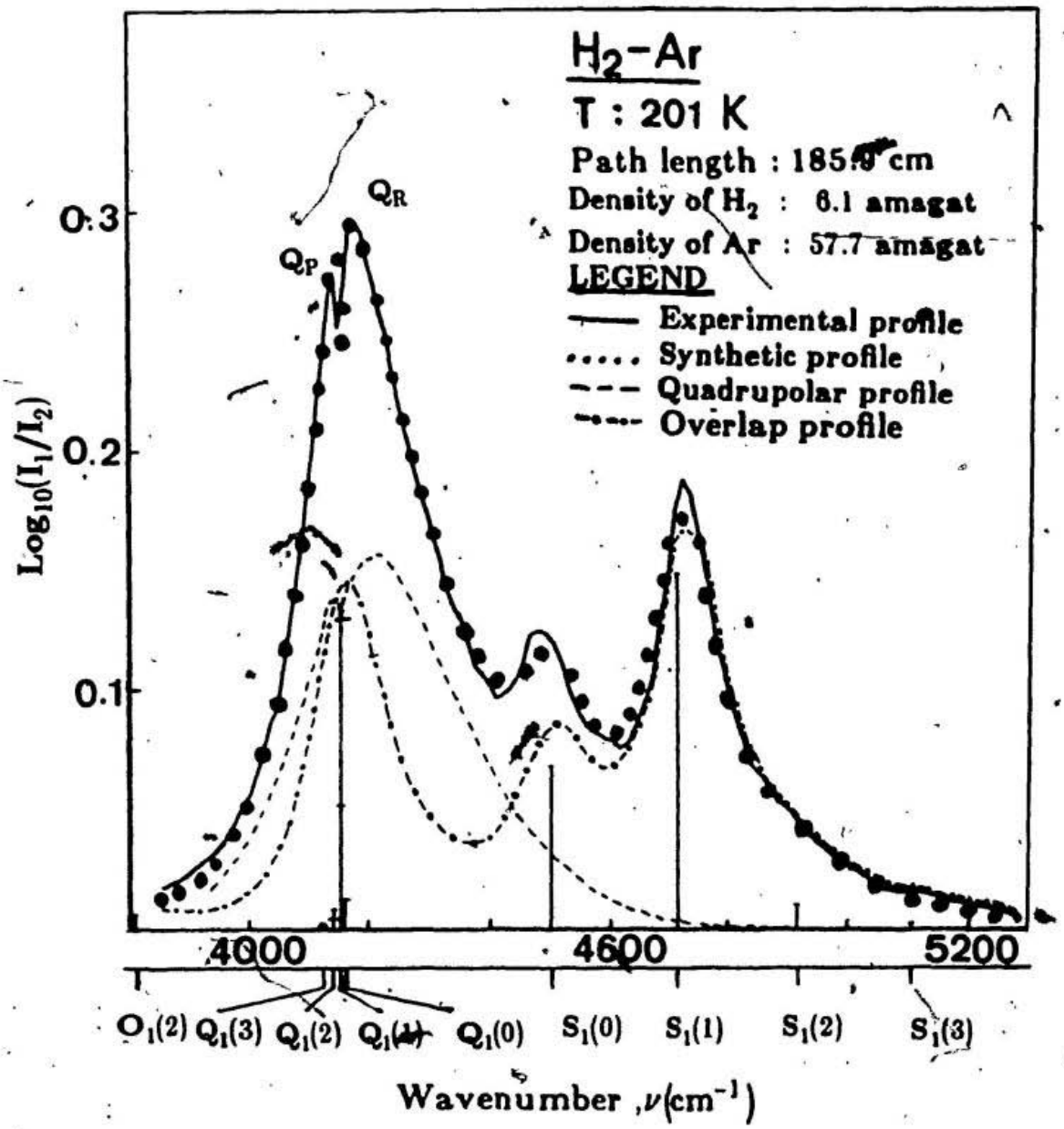

Fig. 18. Analysis of an enhancement absorption profile obtained in a H_2 - Ar binary mixture at 201 K.

Table IV

Results of the profile analysis of H_2-Ar binary mixtures

Temperature T (K)	Intracollisional half-width δ_d (cm^{-1})	collision duration τ_d (10^{-14} s)	Quadrupolar half-width δ_q (cm^{-1})	collision duration τ_q (10^{-14} s)	Overlap contribution %	Quadrupolar contribution %
201	159 ± 4	3.3(3)	75 ± 4	7.1(2)	43	57
273	166 ± 4	3.2(0)	87 ± 4	6.1(4)	42	58
296	168 ± 4	3.1(6)	89 ± 4	6.0(0)	40	60

duration between successive collisions decreases, giving an increase in the separa-

$$\delta_c = a\rho_b + b\rho_b^2 \ , \ (a >> b) \ , \tag{19}$$

where ρ_b is the perturbing gas density and a and b are constants. A plot of δ_c vs ρ_b is shown in Figs. 19 & 20. In Fig. 19, out of total 9 points, the first two corresponding to argon densities less than 50 amagat deviate considerably from the fitted curve, which passes through the origin. The collision diameter σ_{12} and the coefficient a are related by (see Mactaggart and Welsh, 1973, Chapman and Cowling, 1952, and Prasad and Reddy, 1977)

$$a = \frac{(1 - \bar{\Delta})\, \sigma_{12}^2\, n_0}{c\left(\frac{\pi\, m_r}{2kT}\right)^{1/2}} \ , \tag{20}$$

where $\bar{\Delta}$ is the mean persistence - of - velocity ratio, n_0 is the Loschmidt's number defined in Chapter 3, m_r is the reduced mass of the colliding pair, k is the Boltzmann constant, and T is the absolute temperature. The mean persistence - of - velocity ratio, $\bar{\Delta}$ is that given by (Chapman and Cowling, 1952)

$$\bar{\Delta} = \frac{M_1}{2} + \frac{M_1^2}{2\sqrt{M_2}} \ln\left[\frac{\sqrt{M_2} + 1}{\sqrt{M_1}}\right] \ , \tag{21}$$

where $M_1 = m_1/(m_1 + m_2)$ and $M_2 = m_2/(m_1 + m_2)$, m_1 and m_2 being the individual masses of H_2 and Ar molecules respectively. The value of $\bar{\Delta}$ for a mixture of H_2 - Ar obtained in this way is 0.0264 at 273 K and the collision diameter σ_{12} (Å) calculated from a is 2.76 Å, which is slightly less than the Lennard-Jones

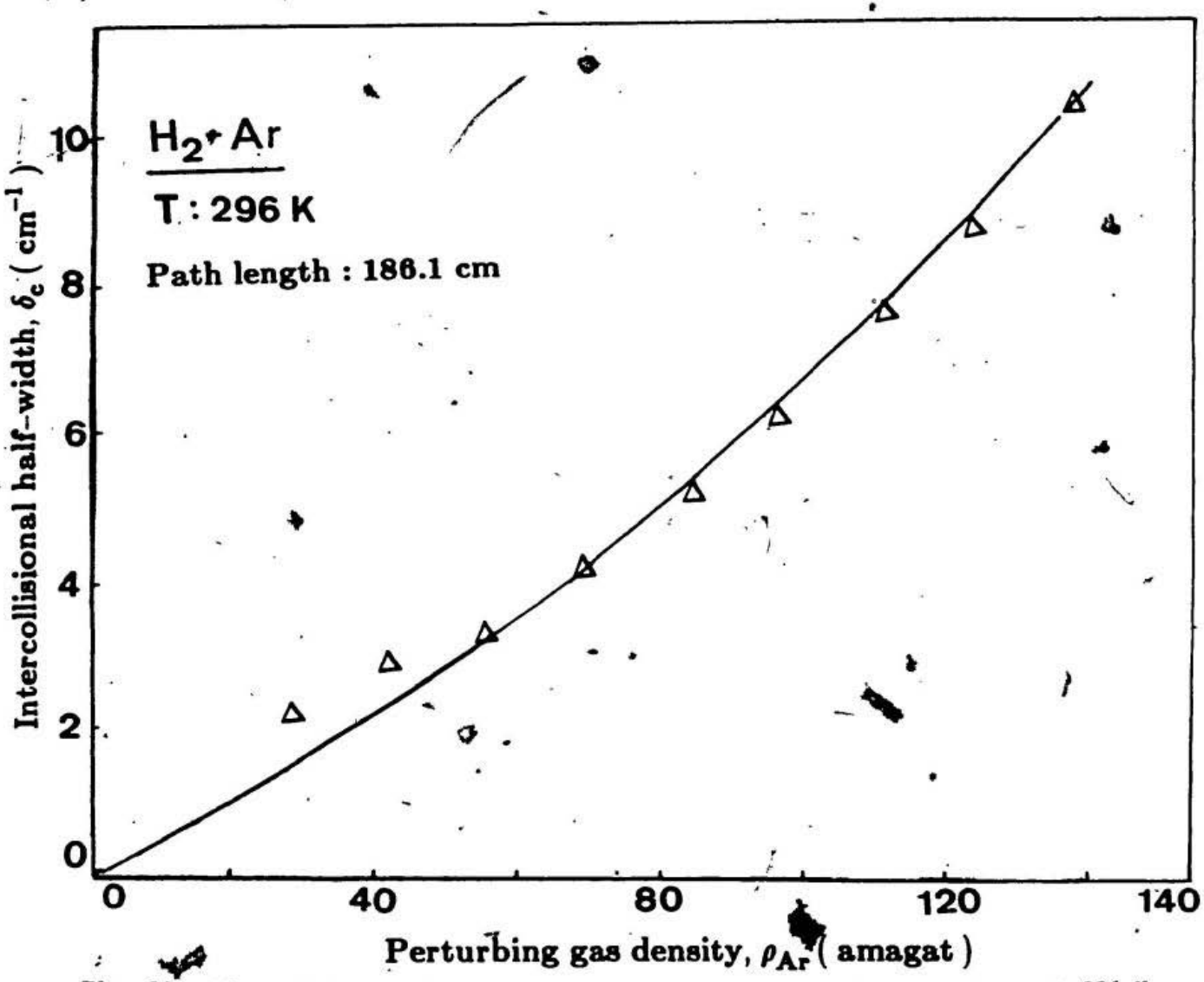

Fig. 19. Plot of intercollisional half-width parameter, δ_c against ρ_b at 296 K.

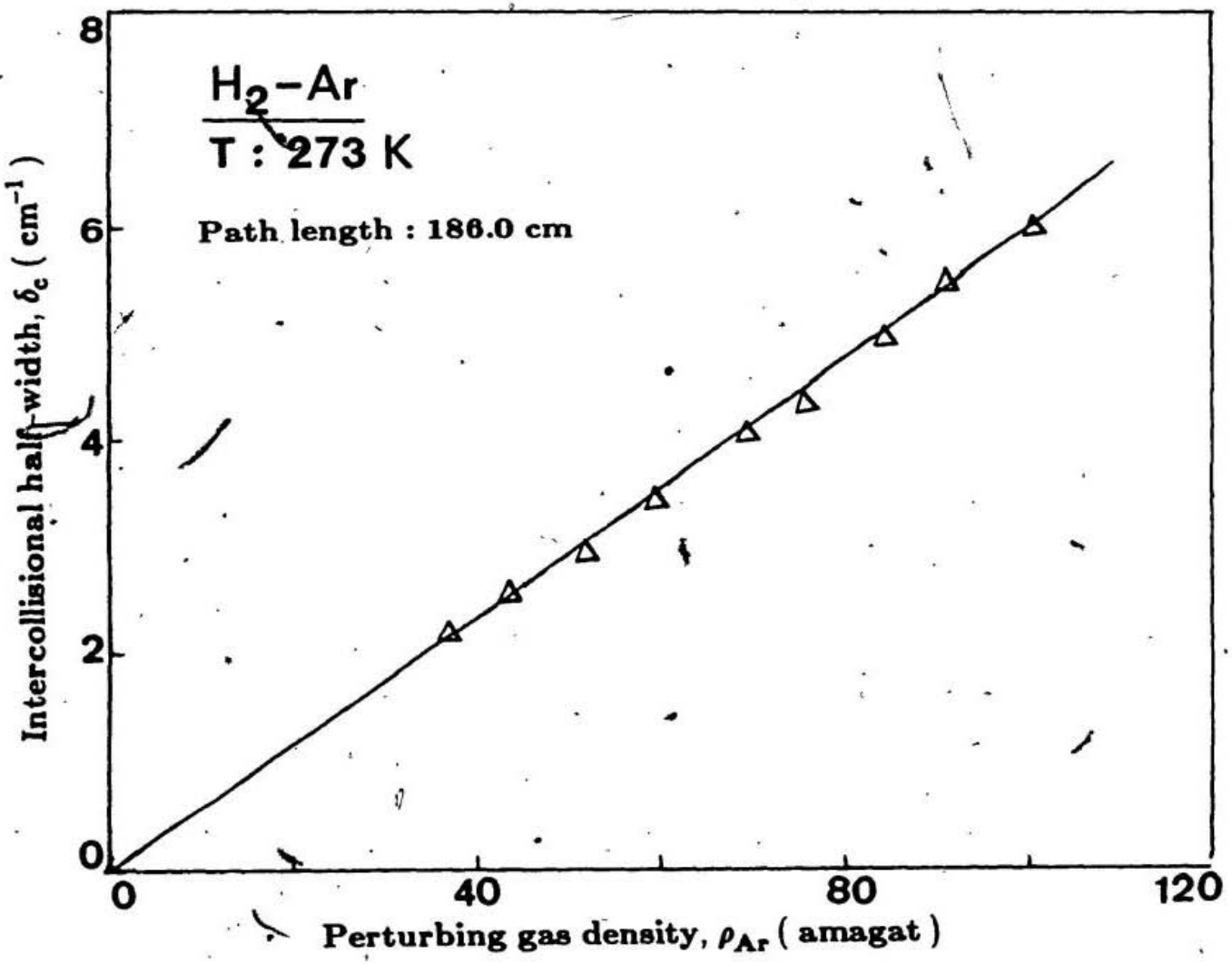

Fig. 20. Plot of intercollisional half-width parameter, δ_c VS. ρ_b at 273 K.

diameter σ_{12}^{LJ}, 3.17 Å.

The temperature dependence of the half-widths δ_d and δ_q is clearly evident from Table IV. As discussed in Chapter 1, page 4, the half-widths of CIA components are in general directly proportional to square root of the absolute temperature. The values of δ_d and δ_q obtained from the profile analysis were plotted against $\sqrt{T}$ in Fig. 21. Assuming the direct proportionality relation between δ_q and $\sqrt{T}$, the δ_q vs $\sqrt{T}$ plot in Fig.21 was constrained to pass through the origin. The quadrupolar half-width δ_q satisfies the linear relation $\delta_q = 5.26\sqrt{T}$ (for H_2–H_2 molecular pairs, $\delta_q = 7.97\sqrt{T}$ (Reddy *et al.*, 1977)). However, the plot of δ_d against $\sqrt{T}$, when extrapolated to $T = 0$ has a value of 116 cm^{-1}. This large value of δ_d corresponding to $T = 0$ can be understood from the fact that the collision duration remains relatively short because the overlap induction takes place in the region of strong repulsive forces, which are operative even at $T = 0$. A similar situation was found to exist in the case of H_2 – H_2 (Reddy *et al.*, 1977), HD – HD (Reddy and Prasad, 1977), D_2 – D_2 (Penney *et al.*, 1982). The intercollisional half-width parameter δ_c also increases with temperature. It is less than 1 cm^{-1} at 201 K, 4.9 cm^{-1} for $\rho_a = 6$ amagat and $\rho_b = 86$ amagat at 273 K, and 6.2 cm^{-1} for $\rho_a = 6$ amagat and $\rho_b = 89$ amagat at 296 K. As the spectral resolution of the monochromator is not enough to resolve the intercollisional dip completely, the intercollisional half-width parameters obtained in this profile analysis may not be very accurate.

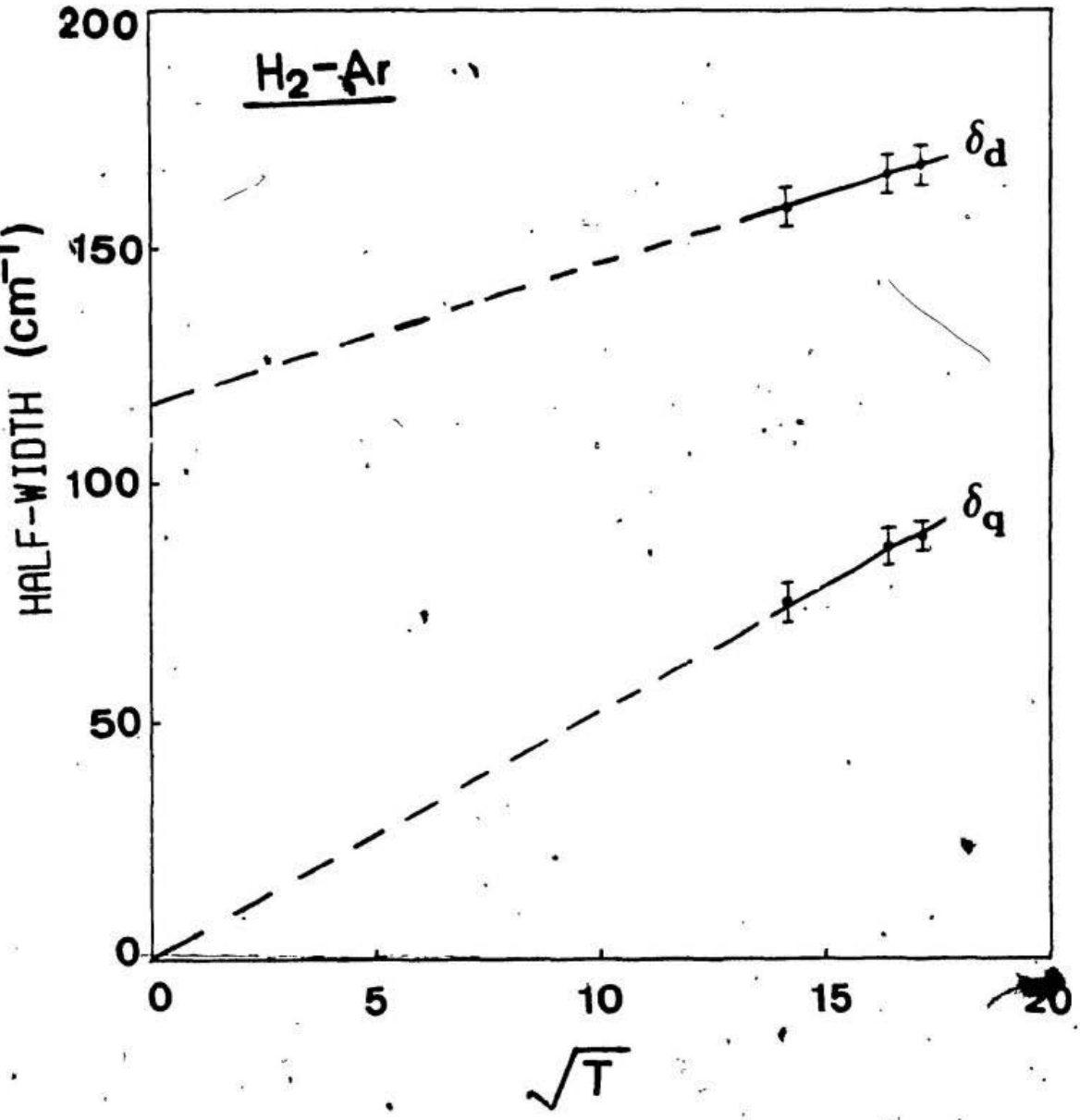

Fig. 21. Plots of half-width parameters δ_d and δ_q against the square root of absolute temperature T (in ^oK).

CHAPTER 5

OVERLAP PARAMETERS FOR THE H_2 - Ar MOLECULAR PAIRS

The contributions to the intensity of the enhancement of the collision-induced fundamental absorption band, resulting from both the overlap- and quadrupole- induced components have been separated in Chapter 4, by the method of profile analysis. The results of the analysis are used in this chapter to determine the overlap parameters λ and ρ, representing the magnitude and range, respectively, of the overlap dipole moment and $\mu(\sigma)$, the overlap-induced dipole moment at the Lennard - Jones intermolecular diameter σ, for the H_2 - Ar collision pairs from the theory of Van Kranendonk (1958).

5.1 The Overlap Absorption Coefficients

The enhancement of the integrated overlap absorption coefficients $\int \alpha_{en(ov)}(\nu)\, d\nu$ obtained from the profile analysis can be represented in terms of its partial densities $\rho_a(=\rho_{H_2})$ and $\rho_b(=\rho_{Ar})$ by the relation

$$\int \alpha_{en(ov)}(\nu)\, d\nu = \alpha_{1b(ov)} \rho_a \rho_b + \alpha_{2b(ov)} \rho_a \rho_b^2 + \cdots \qquad (20)$$

or

$$(1/\rho_1\rho_b) \int \alpha_{en(ov)}(\nu)\, d\nu = \alpha_{1b(ov)} + \alpha_{2b(ov)} \rho_b + \cdots, \qquad (21)$$

where $\alpha_{1b(ov)}$ (cm^{-2} $amagat^{-2}$) and $\alpha_{2b(ov)}$ (cm^{-2} $amagat^{-3}$) are the binary and ternary absorption coefficients, respectively. Plots of $(1/\rho_a\rho_b) \int \alpha_{en(ov)}(\nu)\, d\nu$ vs ρ_b at

temperatures 201, 273, and 296 K are shown in Fig. 22, and are found to have a linear dependence ρ_b. The intercepts and slopes of these plots representing the overlap binary and ternary absorption coefficients, respectively, were obtained by linear least squares fit of the experimental data. The values of these coefficients and those of the new binary absorption coefficients $\tilde{\alpha}_{1b(ov)}$ ($cm^6\ s^{-1}$), obtained by using a relation similar to Eq. (7) are listed in Table V.

5.2 Overlap Parameters for the H_2 - Ar Molecular Pairs

For the fundamental band the overlap binary absorption coefficient $\tilde{\alpha}_{1b(ov)}$ as given by Van Kranendonk (1958) is

$$\tilde{\alpha}_{1b(ov)} = (8\pi^3/3h)k_1^2 \int |\{\vec{M}_{ov}(\vec{R})\}_{ov}|^2 g_o(\vec{R})\, d^3\vec{R}\,, \qquad (22)$$

where $\vec{M}_{ov} = \left(\frac{\partial \vec{\mu}_{ov}}{\partial r}\right)_0$ is the rate of change of the induced overlap dipole moment $\vec{\mu}_{ov}$ with respect to r at the internuclear separation r_0. The quantity $g_0(\vec{R})$ is the low density limit of the pair distribution function, ξ is the matrix element $<0 \mid r - r_0 \mid 1>$ corresponding to $v = 1 \leftarrow v = 0$ and $d^3\vec{R}$ is the volume element. The quantity $M_{ov}(\vec{R})$ is assumed to decrease exponentially with the intermolecular separation R and is expressed as

$$M_0(R) = \xi \exp(-R/\rho) = \lambda e \exp[-(R - \sigma)/\rho]\,. \qquad (23)$$

Here λe is the amplitude of the oscillating overlap induced moment when the molecular separation is σ corresponding to the intermolecular potential $V(\sigma) = 0$. λ is a dimensionless quantity given by

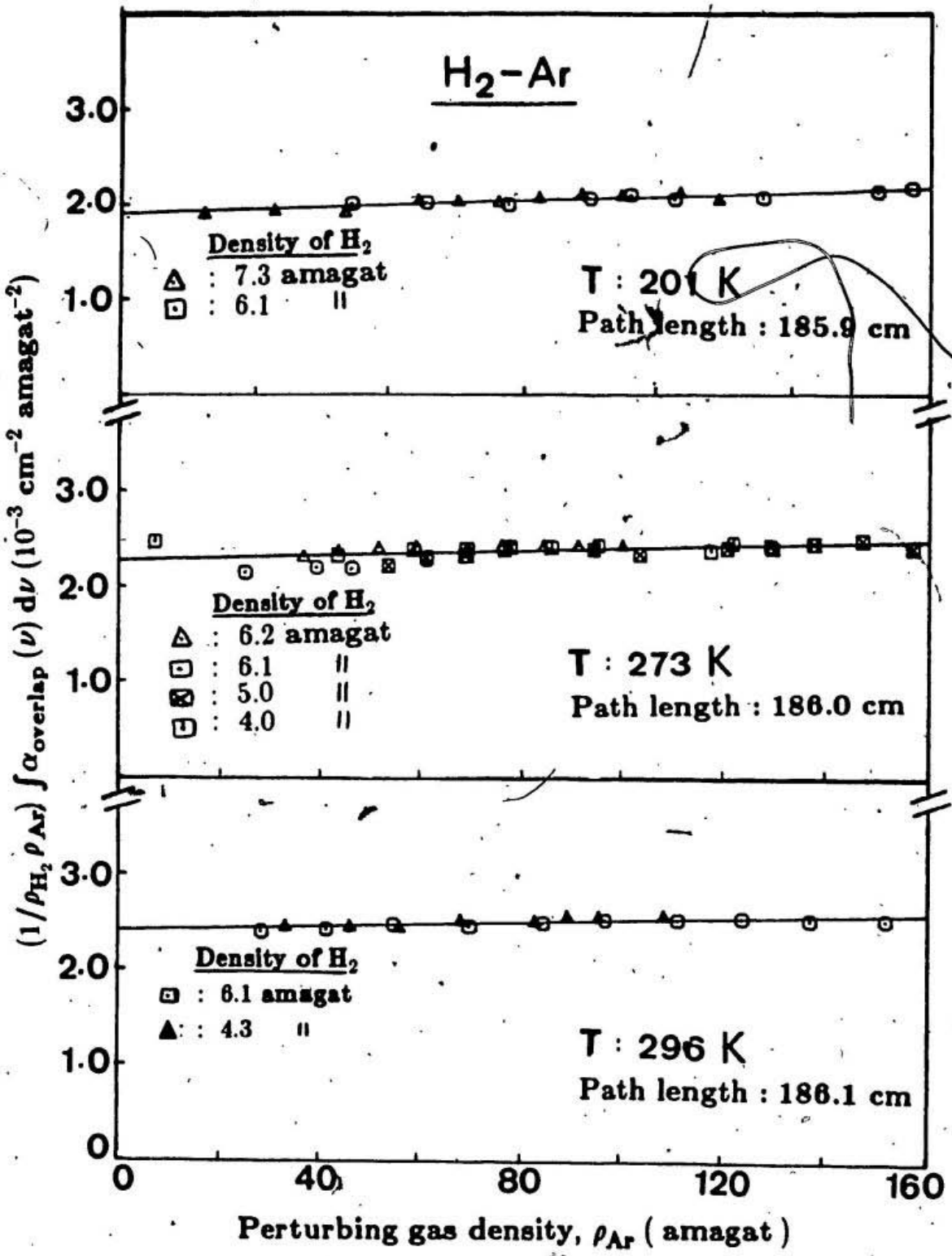

Fig. 22 Plots of $(1/\rho_a\rho_b)\int\alpha_{overlap}(\nu)d\nu$ vs. ρ_b for the overlap enhancement absorption profiles.

TABLE V.

Overlap absorption coefficients[a] of the fundamental band of H_2-Ar binary mixture at 201,273 and 296K.

Temperature T (K)	Binary absorption coefficient α_{1b} (10^{-3} cm^{-2} amagat^{-2})	$\bar{\alpha}_{1b}$ (10^{-35} cm^{-6} s^{-1})	Ternary absorption coefficient α_{2b} (10^{-6} cm^{-2} amagat^{-3})
201	1.90 ± 0.02	1.80 ± 0.02	2.18 ± 0.27
273	2.27 ± 0.03	2.15 ± 0.03	1.34 ± 0.34
296	2.41 ± 0.02	2.28 ± 0.02	1.20 ± 0.22

a) Ranges of error indicated are standard deviations.

$$\lambda = (\xi/e)\exp(-\sigma/\rho)\,, \tag{24}$$

and

$$\mu_{ov}(\sigma) = \lambda e\sigma\,. \tag{25}$$

The quantities ξ and ρ give respectively the magnitude and the range of the oscillating part of the overlap induced moment. Equation (22) can now be written as

$$\tilde{\alpha}_{1b(ov)} = \frac{8\pi^3}{3h} |\,<0\,|\,r - r_0\,|\,1>\,|^2\,\lambda^2 e^2\sigma^3 4\pi \int_0^\infty e^{-2(R-\sigma)/\rho}\, g_0(R)\, 4\pi R^2\, dR$$

$$= \lambda^2 I\tilde{\gamma}\,, \tag{26}$$

where $\tilde{\gamma}$ is given by

$$\tilde{\gamma} = (8\pi^3/3h\; e^2\sigma^3)\;|\,<0\,|\,r - r_0^2\,|\,1>\,|\,, \tag{27}$$

which has the dimensions of the binary absorption coefficient. The temperature-dependent dimensionless integral $I(T^*)$ is given by

$$I(T^*) = 4\pi \int_0^\infty e^{-2(x-1)\sigma/\rho}\, g_0(x)\, x^2\, dx\,, \tag{28}$$

where $x = R/\sigma$ and $g_0(x)$ is the classical pair distribution function given by

$$g_0(x) = \exp[-V^*(x)/T^*]\,. \tag{29}$$

Here T^* $(= kT/\epsilon)$ is the reduced temperature and $V^*(x)$ $(= V(x)/\epsilon)$ is the reduced intermolecular potential, ϵ being the depth of the potential. In this work Lennard-Jones intermolecular potential is assumed and is given by

$$V(x) = 4\epsilon(x^{-12} - x^{-6})\,, \tag{30}$$

At intermediate temperatures, where quantum effects should be included, the integral I can expressed as

$$I = I_{cl} - \Lambda^{*2} I^{(2)} + \Lambda^{*4} I^{(4)} + \cdots, \qquad (31)$$

where

$$\Lambda^* = \left[\frac{h^2}{2m_{00}\epsilon\sigma^2}\right]^{1/2} \qquad (32)$$

is the reduced de Broglie wavelength. Here m_{00} is the reduced mass of the colliding pair of molecules. The values of the depth of the Lennard - Jones potential $\epsilon = 66.58\,^{\circ}K$ and the Lennard - Jones diameter $\sigma = 3.167$ Å were taken from Hirschfelder *et al.*, (1967), who calculated these parameters using the empirical combining laws, ie., $\sigma_{12} = \frac{1}{2}(\sigma_1 + \sigma_2)$ and $\epsilon_{12} = \sqrt{\epsilon_1 \epsilon_2}$, as the force constants for a dissimilar pair of molecules are not available. The force constants obtained in this way seem to give reasonably good results in calculations involving mixtures (see Hirschfelder *et al.*, pages 168, 169 and 222). The matrix element $<0 \mid r - r_0 \mid 1>$ were obtained from Poll (1975). For H_2 - Ar molecular pairs $\Lambda^* = 0.8678$ and $\tilde{\gamma} = 7.09 \times 10^{-32}$($cm^6\ s^{-1}$). The experimental values of $\lambda^2 I$ for the H_2 - Ar pairs were obtained from Eq. (26), from the observed $\tilde{\alpha}_{1b(ov)}$ and the calculated $\tilde{\gamma}$ and were plotted against the absolute temperature T in Fig. 22. The integral I_{cl} (Eq. (28)) depends on the factors σ/ρ and T^*. In order to find the most probable value of σ/ρ for H_2 - Ar pairs, the integral I_{cl} was computed for a series of values of ρ/σ in the range 0.070 to 0.140 at intervals of 0.002 at the,

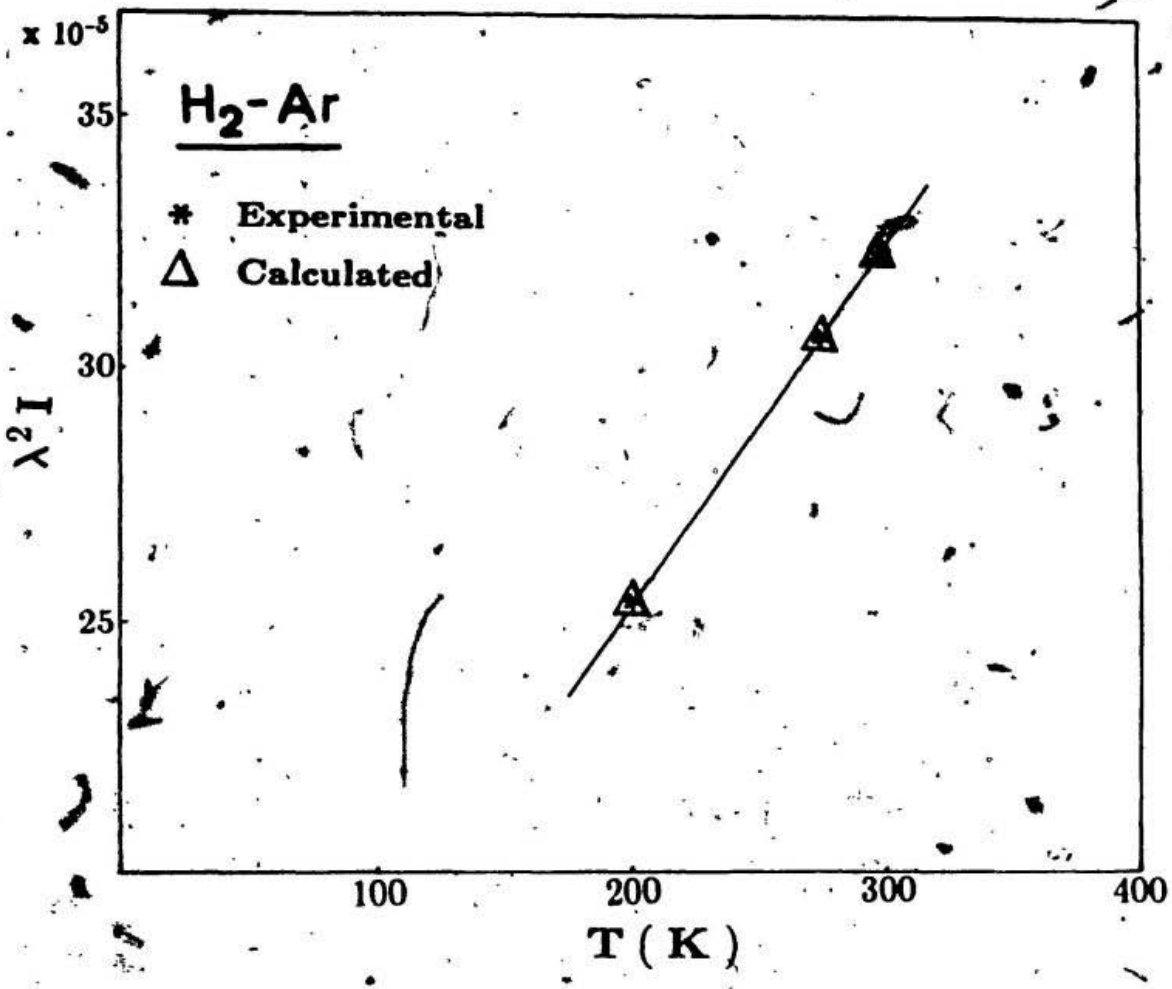

Fig. 23. Variation of $\lambda^2 I$ against absolute temperature (T).

experimental temperatures T^*. The quantum corrections $I^{(2)}$ and $I^{(4)}$ were obtained from Gibbs *et al.* (1979). Finally the appropriate values of I were obtained from Eq. (31). The quantity λ^2, assumed to be independent of temperature, was obtained from the values of $\lambda^2 I$, at the three experimental temperatures for a particular value of ρ/σ using the corresponding value of I. It was found that for the value of $\rho/\sigma = 0.104$ for H_2 – Ar, the λ^2 values obtained at the three experimental temperatures were such that the $\sum\delta_i^2$ where δ_i are the deviations of the calculated values of $\lambda^2 I$ from the corresponding experimental values was a minimum. The experimental and calculated values of $\lambda^2 I$ against T are plotted in Fig. 22. The values of ρ/σ and λ for H_2 – Ar pairs obtained from this fit are listed in Table VI. The values of ρ, σ, and $\mu_{ov}(\sigma)$, the induced dipole moment corresponding to the Lennard-Jones diameter σ, are also listed in the same table. The corresponding values for the molecular pairs H_2 – H_2 (Reddy *et al.*, 1977), H_2 – He and H_2 – Ne (Reddy and Chang, 1973) are also listed in this table for comparison.

TABLE VI

Overlap parameters for the H_2-H_2, H_2-He, H_2-Ne and H_2-Ar pairs.

Collision pair	ρ/σ	λ (10^{-2})	σ (A^0)	ρ (A^0)	$\mu_{overlap}(\sigma)$ (10^{-2} ea_o)	Reference
H_2-H_2	0.071	0.37	2.928	0.21	2.00	Reddy et al. (1977a)
H_2-He	0.088	0.56	2.757	0.24	2.9	Reddy & Chang (1973)
H_2-Ne	0.100	0.90	2.854	0.29	4.9	Reddy & Chang (1973)
H_2-Ar	0.104	1.01	3.167	0.33	6.05	Present work

CHAPTER 6

HEXADECAPOLE - INDUCED U TRANSITIONS IN H_2 - Ar MIXTURES

6.1 Introduction

The results of a systematic study of the CIA of the fundamental band of H_2 in H_2 – Ar mixtures arising from the overlap and quadrupolar induction mechanisms have been presented in Chapters 3, 4, and 5. The dipole induced in an Ar atom by the hexadecapole field of its colliding partner H_2 give rise to the rotational selection rule $\Delta J = 0, \pm 2, \pm 4$. The small magnitude of the hexadecapole moment of H_2 results in relatively weak transitions. The hexadecapole-induced U transitions of the form $U_1(J)$ and $Q_1(J) + U_0(J)$ corresponding to the rotational selection rule $\Delta J = +4$, first observed in the pure H_2 at 195 K by Gibbs *et al.* (1974) were later studied in more detail at 77 K by Reddy *et al.* (1980), who analyzed the observed profiles using the theoretical matrix elements of the hexadecapole moment of H_2, calculated numerically by Karl *et al.* (1975). The U transitions in the fundamental band of solid H_2 both in normal and para species have also been first observed in our laboratory by Prasad *et al.* (1978). However, prior to the present work, no U transitions have been observed in the fundamental band of H_2 in any binary mixture of H_2 with foreign gases. In this chapter we report the observation of U branch transitions in the fundamental

band H_2 in H_2 - Ar mixtures at 296 K and this constitutes the first such observation in a H_2 – foreign gas mixture.

6.2 Observation of U Transitions in H_2 – Ar Mixtures.

The experiment to observe the $U_1(1)$ transition was performed with the 2 m high-pressure stainless steel absorption cell and other experimental apparatus described in Chapter 2. The slit-width, maintained at 45 μm, of the Perkin-Elmer model 99 double pass monochromator equipped with an LiF prism, gave a spectral resolution of $\sim$9 cm^{-1} at 5695 cm^{-1}, the calculated wavenumber of the $U_1(1)$ transition. The enhancement absorption spectra were recorded at 296 K with a base density of 59.7 amagat of H_2 for several partial densities of Ar in the range 350 - 520 amagat. Three representative enhancement absorption profiles of the fundamental band of H_2 in the spectral region 5300 – 6200 cm^{-1} for argon gas densities of 438, 491, and 519 amagat are presented in Fig. 24. The position of the $U_1(1)$ (5695.6 cm^{-1}) calculated from the constants for the free H_2 molecule (Stoicheff, 1957) is shown on the wavenumber axis. As mentioned earlier, double transitions of the type $Q_1(J) + U_0(J)$ do not occur in the enhancement absorption spectra of H_2 – Ar mixtures. The single transition $U_1(0)$ which is expected to occur at 5271.6 cm^{-1} is completely masked by the strong absorption in the wings of the overlap and quadrupolar components of the fundamental band. The other U branch transitions, namely, $U_1(2)$ and $U_1(3)$ are too weak to observe. The observations reported in this chapter are only preliminary. Further work on the U branch transitions in H_2 – Ar mixtures at lower temperatures is planned for

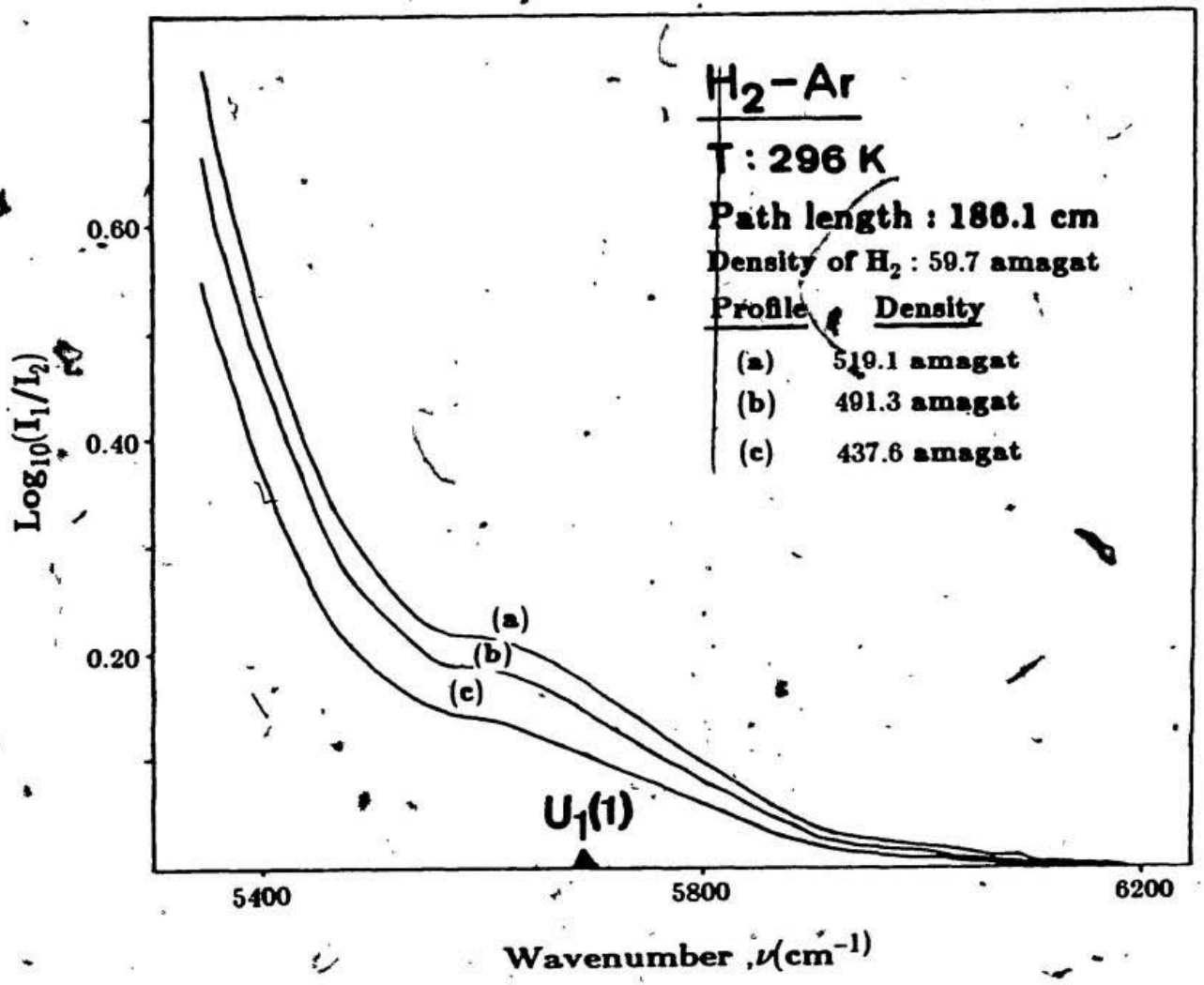

Fig. 24. Hexadecapole-induced $U_1(1)$ transition in H_2-Ar mixtures at 296 K.

the future. Once an accurate set of enhancement absorption profiles at lower temperatures is obtained, absorption due to U branch transitions will be separated from that of the other transitions by the method of profile analysis used by Reddy *et al.* (1980) for their work on the U branch transitions in the pure H_2 gas at 77 K.

The half-width parameters of the collision-induced quadrupolar lines have shown density dependence at high densities. De Remigis *et al.* (1971) observed a decrease in the half-widths of the quadrupolar S lines in the fundamental band of H_2 in H_2 – Ar mixtures at 152 K for gas densities above 300 amagat. This line narrowing was explained by Zaidi and Van Kranendonk (1971) in terms of a diffusional effect in which the line width is proportional to the diffusion constant, which, in other words, is approximately proportional to the density of the gas. However, Lewis and Tjon (1978) showed that this explanation is inapplicable in some cases. Mactaggart *et al.* (1973) studied this pressure narrowing in more detail for the quadrupolar lines of the fundamental band of H_2 in H_2 – Ar, H_2 – Kr, and H_2 – Xe. As the $U_1(1)$ in H_2 – Ar in the present work was observed for densities above 300 amagat it is quite possible that this pressure narrowing effect may be present in this transition also. However, definite conclusions in this regard will be possible only after a satisfactory analysis of the absorption profiles obtained in the present work as well as of the profiles to be obtained at other temperatures in the future.

CHAPTER 7

CONCLUSIONS

In the present experimental project several modifications to the data acquisition system designed by Gillard (1983), have been made. In particular, a microprocessor controlled dc stepping motor was successfully incorporated into the spectrometer system in the place of a continuous drive, which had been used by earlier researchers in our laboratory. The control unit for the stepping motor was initially designed by Gillard (1986) and was assembled in the present work. The spectral region was calibrated against the pulse numbers of the stepping motor and the signal corresponding to the absorption profiles was digitized at each step of the motor by using an analog to digital converter system. This new arrangement helped in analysing the experimental data with a reasonably good accuracy and repeatability without undergoing the manual labor involved in measuring the intensities of the absorption profiles, at different wavenumbers. In order to begin the recording of the absorption profiles accurately at a particular point, two optical switches were fixed to the body of the monochromator (see Sec. 2.8) and the microcomputer was programmed to read the optical switches at each step of the motor.

Also, some modifications were made to the 2 m stainless steel, high-pressure and low-temperature absorption cell in order to prevent the O-ring R_2 (Fig. 2)

from freezing at low-temperatures, which in turn affects the vacuum tight seal of the vacuum chambers provided at each end of the cell. This was achieved by welding the outer bellows (B_1) to a flange F_3 (Fig. 2), which is larger in diameter to the previous one, and by increasing the distance of O-ring R_2 from the cold cell. Thus, cell windows were free from the atmospheric water vapour and improved operating conditions for the cell, were obtained, particularly at low-temperatures.

The collision induced absorption enhancement spectra of the fundamental band of H_2 in H_2 – Ar mixtures at 201, 273 and 296 K were recorded for a total of 88 densities. From the analysis of these spectra several parameters have been determined for the H_2 – Ar mixtures. These are the absorption coefficients: α_{1b}, α_{2b}, $\tilde{\alpha}_{1b}$, $\alpha_{(ov)1b}$, $\alpha_{(ov)2b}$ and $\tilde{\alpha}_{(ov)1b}$ (Table 2 and Table 5), the overlap half-width parameters: δ_c and δ_d (Table 4), and the quadrupolar half-width parameter δ_q (Table 4). From the absorption coefficients it was found that the main contribution to the CIA spectra at all experimental temperatures arose from the binary collisions and the contribution from the ternary collisions is relatively small. The quadrupolar and overlap half-width parameters decreased approximately linearly with $\sqrt{T}$. The half-width δ_c of the intercollisional interference dip, increased with the perturbing gas density ρ_b and was represented by the expression $\delta_c = a\,\rho_b + b\,\rho_b^2$. The collision diameter σ_{12} calculated from the linear coefficient a is about 12 % less than the Lennard - Jones diameter σ_{12}^{LJ} for the H_2 – Ar molecular pairs. The overlap parameters: ρ, λ, and $\mu_{ov}(\sigma)$ (Table 6), were calcu-

lated for the H_2 – Ar molecular pairs for the first time in the present research project.

The experiments carried out on the fundamental band of H_2 in H_2 – Ar mixtures for higher densities upto 520 amagat at 296 K have shown the occurence of the $U_1(1)$ transition corresponding to the selection rule $\Delta J = +4$. This is the first observation of the U branch transition in a H_2 – foreign gas mixture.

APPENDIX A

Program to Control the Peripheral Devices of the Data Acquisition System

PROGRAM TO CONTROL THE MICROPROCESSOR

```
010 REM DATA LOGGER
020 FW = 0
030 BACK = 1
040 DELAY = 2000
050 STIME = 100
060 INPUT "INITIAL TRACE NO.";G
070 OUT 11,146
080 OUT 10,255
090 REM READ FILENAME,TEMP,PATH LENGTH
100 READ F$,H$,T,PT
110 PRINT "POSITION SPECTROMETER - F FOR FORWARD"
120 PRINT "    B FOR BACKWARD"
130 PRINT "    <CR> TO CONTINUE IN THE SAME DIRECTION"
140 PRINT "    Q TO START LOGGING DATA"
150 OUT 11,FW
160 INPUT A$
170 IF A$ = "F" THEN OUT 11,1
180 IF A$ = "B" THEN OUT 11,0
190 IF A$ = "Q" THEN GOTO 310
200 OUT 11,3 : OUT 11,2
210 GOSUB 1950
220 PRINT INP(9);
230 GOTO 160
```

```
240 REM SET INITIAL VALUE
250 PRINT "SET INITIAL VALUE"
255 PRINT "     Q - TO CONTINUE"
257 PRINT "     J - TO SET THE VALUE"
260 OUT 11,146
270 GOSUB 1500
280 PRINT E
290 INPUT A$ : IF A$ <> "Q" GOTO 260
310 PRINT "SWITCH TO VAX, THEN PRESS RETURN" : INPUT A$
320 PRINT "sed -f ed.file > ";F$+MID$(STR$(G),2)
330 GOSUB 1900
340 REM GET INITIAL DATA
350 PRINT H$
360 PRINT "TRACE NO.";G
370 INPUT "PRESSURE";P
380 INPUT "NO. OF POINTS";N
390 PRINT "DENSITY";O
395 PRINT "NO. OF POINTS";N
400 PRINT "PATH LENGTH";PT
410 PRINT "TEMPERATURE";T
420 REM INITIALIZE TIMERS, ADC, ETC.
430 REM INITIALIZE PPI
440 OUT 11,146
450 REM DISABLE ADC OUTPUT
460 OUT 11,8 : OUT 11,10 : OUT 11,12
470 REM SET MOTOR TO STEP FORWARD
```

```
480 OUT 11,FW
490 REM SET UP TIMERS FOR 0 AVERAGE
500 OUT 7,54 : OUT 7,116
510 REM CLOSE SHUTTER
520 REM GET ZERO AVERAGE
530 OUT 11,15
540 REM START FAST TIMER
550 OUT 4,24 : OUT 4,0
560 REM START 0.5 SEC. TIMER
570 OUT 5,0 : OUT 5,125
580 S=0
590 FOR I=1 TO 40
600 GOSUB 1400
610 S=S+E
620 NEXT I
630 S=INT(S/40+.5)
640 PRINT "0 AVERAGE ";S
650 REM OPEN SHUTTER
660 OUT 11,14
700 REM SET UP FOR DATA COLLECTION
710 REM INITIALIZE TIMERS
720 OUT 7,116 : OUT 7,176
730 REM START 0.5 SEC. INTERVAL TIMER
740 OUT 5,0 : OUT 5,125
750 REM SET UP COUNTER FOR INTERVALS
760 OUT 6,0 : OUT 6,250
```

```
800 REM START SAMPLING EVERY INTERVAL
810 FOR I=1 TO N
820 REM GET DIGITIZED VALUES AS E
830 GOSUB 1400
840 Z=INP(9) : Z = Z-INT(Z/64)*64
850 PRINT K;E-S;Z
860 REM STEP MOTOR
870 OUT 11,3 : OUT 11,2
880 NEXT I
890 PRINT "COMMENT/2 LINES"
900 INPUT A$ : INPUT A$
1000 REM PLACE DATA IN FILE AND REPOSITION SPECTROMETER
1010 PRINT CHR$(4)
1020 GOSUB 1900
1030 REM START NEXT RUN
1040 REM REWIND DRUM
1050 OUT 11,BACK
1060 FOR I = 1 TO N + 20
1070 GOSUB 1950
1080 OUT 11,3 : OUT 11,2
1090 NEXT I
1100 GOSUB 1910
1110 OUT 11,FW
1120 FOR I = 1 TO 20
1130 GOSUB 1950
1140 OUT 11,3 : OUT 11,2
```

```
1150 NEXT I
1160 G = G+1
1170 GOTO 110
1200 DATA "file"
1210 DATA"TITLE"
1230 DATA 298
1240 DATA 186.1
1250 END
1400 REM READ ADC , RETURNS A
1420 OUT 7,64
1430 X=INP(5) : X=INP(5)
1440 Y=X
1450 OUT 7,64
1460 X=INP(5) : X=INP(5)
1470 IF X<Y THEN 1440
1500 REM ONE INTERVAL HAS PASSED
1510 WAIT 8,64
1520 OUT 11,10 : OUT 11,8
1530 Z=INP(8)
1540 A=Z-INT(Z/16)*16
1550 OUT 11,10 : OUT 11,9
1560 Z=INP(8)
1570 B=Z-INT(Z/16)*16
1580 OUT 11,11 : OUT 11,8
1590 Z= INP(8)
1600 C=Z-INT(Z/16)*16
```

```
1610 OUT 11,11 : OUT 11,9
1620 Z=INP(8)
1630 D=Z-INT(Z/16)*16
1640 OUT 7,128
1650 L=INP(6)+256*INP(6)
1660 K=64000-L
1670 E=A+10*B+100*C+1000*D
1690 RETURN
1900 REM DELAY TIMER
1910 FOR J=1 TO DELAY
1920 NEXT J
1930 RETURN
1950 FOR J = 1 TO STIME
1960 NEXT J
1970 RETURN
1990 END
```

REFERENCES

Birnbaum, A. and Poll, J.D., J. Atmos. Sci., **26**, 943, (1969).

Birnbaum, G. and Cohen, E.R., Can. J. Phys., **54**, 593, (1976).

Birnbaum, G., Guillot, B. and Bratos, S., Adv. Chem. Phys., **51**, 49, (1982).

Chapman, S. and Cowling, T.G., "The Mathematical Theory of Non-Uniform Gases", 2 nd edition, Cambridge University Press, Cambridge, England, (1952).

Chisholm, D.A., MacDonald, J.C.F., Crawford, M.F., and Welsh, H.L., Phys. Rev., **88**, 957, (1952).

Chisholm, D.A. and Welsh, H.L., Can. J. Phys., **32**, 291, (1954).

Crawford, M.F., Welsh, H.L., and Locke, J.L., Phys. Rev., **75**, 1607, (1949).

Crawford, M.F., Welsh, H.L., MacDonald, J.C.F., and Locke, J.L., Phys. Rev., **80**, 469, (1950).

De Remigis, J., Mactaggart, J.W., and Welsh, H.L. Can. J. Phys. **49**, 381 (1971)

Downie, A.R., Magoon, M.C., Purcell, T. and Crawford, B., J. Opt. Soc. Amer., **43**, 941, (1953).

Gibbs, P.W. Gray, C.G. Hunt, J.L. Reddy, S.P. Tipping, R.H. and Chang, K.S., Phys. Rev. Lett., **33**, 256, (1974).

Gibbs, P.W., Hunt, J.L. and Poll, J.D., Can. J. Phys., **57**, 981, (1979).

"IUPAC Tables of Wavenumbers of Calibration of Infrared Spectrometers", (edited by Cole, A.R.H., Pergamon, Oxford-New York, 2nd edition), (1977).

Gillard, P.G., Ph.D. Thesis, Memorial University of Newfoundland, St. John's, Newfoundland, unpublished (1983).

Gillard, P.G., Private Communication, (1986).

Gillard, P.G., Prasad, R.D.G. and Reddy, S.P., J. Chem. Phys., **81**, 3458, (1984).

Hare, W.F.J. and Welsh, H.L., Can. J. Phys., **36**, 88, (1958).

Hirschfelder, J.O., Curtiss, C.F. and Bird, R.B., "Molecular Theory of Gases and Liquids", 4 th edition, John Wiley & Sons,INC. New York, 1967.

Humphreys, C.J., J. Opt. Soc. Amer., **43**, 1027, (1953).

Hunt, J.L. and Welsh, H.L., Can. J. Phys., **42**, 873, (1964).

Hunt, J.L. and Poll, J.D., Molecular Physics, (in press 1986).

Karl, G. and Poll, J.D., J. Chem. Phys., **46**, 2944, (1967).

Karl, G., Poll, J.D. and Wolniewicz, L., Can. J. Phys., **19**, 1781, (1975).

Kiss, Z.K. and Welsh, H.L., Can. J. Phys., **37**, 1249, (1959).

Levine, H.B. and Birnbaum, G., Phys. Rev., **154**, 172, (1967).

Lewis, J.C. and Van Kranendonk, J., Phys. Rev. Lett., **24**, 802, (1971).

Lewis, J.C. and Van Kranendonk, J., Can. J. Phys., **50**, 352, (1972).

Lewis, J.C. and Van Kranendonk, J., Can. J. Phys., **50**, 2881, (1972).

Lewis, J.C. and Van Kranendonk, J., Can. J. Phys., **50**, 2902, (1972).

Lewis, J.C., Physica, **82A**, 500, (1976).

Lewis, J.C., and Tjon, J.A., Physica A, **91**, 191, (1978).

Lewis, J.C. Can. J. Phys., **61**, 440, (1983).

Lewis, J.C. in "Phenomena Induced by Intermolecular Interactions", edited by Birnbaum, G., (Plenum, New York, 1985).

Mactaggart, J.W. and Hunt, J.L., Can. J. Phys., **47**, 65, (1969).

Mactaggart, J.W., and Welsh, H.L., Can. J. Phys., **51**, 158, (1973).

Mactaggart, J.W., De Remigis, J., and Welsh, H.L., Can. J. Phys., **51**, 1971, (1973).

McKellar, A.R.W. and Oka, T., Can. J. Phys., **56**, 1315, (1978).

Michels, A., Wijker, HUB. and Wijker, HK., Physica, **15**, 627, (1949).

Michels, A., Levelt, J.M. and DeGraff, W., Physica, **24**, 659, (1958).

Michels, A., DeGraff, W., Wassenaar, T., Levelt, J.M.H. and Louwerse, P., Physica, **25**, 25, (1959).

Penney, R.J., M.Sc. Thesis, Memorial University of Newfoundland, St. John's, Newfoundland, unpublished (1980).

Penney, R.J., Prasad, R.D.G. and Reddy, S.P., J. Chem. Phys., **77**, 131, (1982).

Plyer, E.K., Gailar, N.M. and Wiggins, T.A., J. Res. Natl. Bur. Standards, **48**, 221, (1952).

Poll, J.D., "Proceedings I.A.U. Symposium 40 on Planetary Atmospheres (Reidel, Dordrecht), 384, (1971).

Poll, J.D., Hunt, J.L. and Mactaggart, J.W., Can. J. Phys., **53**, 954, (1975).

Poll, J.D. and Hunt, J.L., Can. J. Phys., **59**, 1448, (1981).

Poll, J.D., Private Communications, (1983).

Prasad, R.D.G., Ph.D. Thesis, Memorial University of Newfoundland, St. John's, Newfoundland, unpublished (1976).

Prasad, R.D.G. and Reddy, S.P., J. Chem. Phys., **66**, 707, (1977).

Prasad, R.D.G. Clouter, M.J. and Reddy, S.P., Phys. Rev. A., **17**, 1690, (1978).

Reddy, S.P. and Cho, C.W., Can. J. Phys., **43**, 793, (1965).

Reddy, S.P. and Kuo, C.Z., J. Mol. Spectrosc., **37**, 327, (1971).

Reddy, S.P. and Chang, K.S., J. Mol. Spect., **47**, 22, (1973).

Reddy, S.P., Sen, A. and Prasad, R.D.G., J. Chem. Phys., **72**, 6102, (1980).

Reddy, S.P., Varghese, G. and Prasad, R.D.G., Phys. Rev. A., **15**, 975, (1977).

Reddy, S.P. in "Phenomena Induced by Intermolecular Interactions" edited by Birnbaum, G., (Plenum, New York, 1985).

Rich, N.H. and McKellar, A.R.W., Can. J. Phys., **54**, 486, (1976).

Sen, A. M.Sc. Thesis, Memorial University of Newfoundland, St. John's, Newfoundland, unpublished (1978).

Stoicheff, B.P., Can. J. Phys., **35**, 730, (1957).

Varghese, G., Ghosh, S.N., and Reddy, S.P., J. Mol. Spect., **41**, 291, (1972).

Van Kranendonk, J., Physica, **23**, 825, (1957).

Van Kranendonk, J., Physica, **24**, 347, (1958).

Van Kranendonk, J., Can. J. Phys., **46**, 1173, (1968).

Van Kranendonk, J., Physica, **73**, 156, (1974).

Watanabe, A. and Welsh, H.L., Can. J. Phys., **43**, 818, (1965).

Watanabe, A., Can. J. Phys., **49**, 1320, (1971).

Watanabe, A., Hunt, J.L. and Welsh, H.L., Can. J. Phys., **49**, 860, (1971).

Welsh, H.L., Crawford, M.F. and Locke, J.L., Phys. Rev., **76**, 580, (1949).

Welsh, H.L., Crawford, M.F., MacDonald, J.C.F. and Chrisholm, D.A., Phys.

Rev., 83, 1264, (1951).

Welsh, H.L., "MTP International Review of Science, Physical Chemistry", Vol.3, Spectroscopy, edited by Ramsay D.A., (Butterworths, London, 1972).

Zaidel, A.N., Prokofer, V.K., Raisku, S.M., Slavnyi, V.A. and Shreider, E.Ya., "Tables of Spectral Lines" (IFI/Plenum, New York - London), (1970).

Zaidi, H.R. and Van Kranendonk, J., Can. J. Phys., 49, 385, (1971).